HHS Public Access

Author manuscript

Sci Transl Med. Author manuscript; available in PMC 2021 April 19.

Published in final edited form as:

Sci Transl Med. 2018 July 04; 10(448): . doi:10.1126/scitranslmed.aan4470.

MEK inhibition induces MYOG and remodels super-enhancers in RAS-driven rhabdomyosarcoma

Marielle E. Yohe[1,2,*,†], **Berkley E. Gryder**[1,†], **Jack F. Shern**[2], **Young K. Song**[1], **Hsien-Chao Chou**[1], **Sivasish Sindiri**[1], **Arnulfo Mendoza**[2], **Rajesh Patidar**[1], **Xiaohu Zhang**[3], **Rajarashi Guha**[3,‡], **Donna Butcher**[4], **Kristine A. Isanogle**[5], **Christina M. Robinson**[5], **Xiaoling Luo**[6], **Jin-Qiu Chen**[6], **Ashley Walton**[1], **Parirokh Awasthi**[5], **Elijah F. Edmondson**[4], **Simone Difilippantonio**[5], **Jun S. Wei**[1], **Keji Zhao**[7], **Marc Ferrer**[3], **Craig J. Thomas**[3], **Javed Khan**[1,*]

[1]Oncoqenomics Section, Genetics Branch, National Cancer Institute, National Institutes of Health (NIH), Bethesda, MD 20892, USA.

[2]Pediatric Oncology Branch, National Cancer Institute, NIH, Bethesda, MD 20892, USA.

[3]Division of Preclinical Innovation, National Center for Advancing Translational Sciences, NIH, Bethesda, MD 20892, USA.

[4]Pathology/Histotechnology Laboratory, Leidos Biomedical Research Inc., Frederick National Laboratory for Cancer Research, NIH, Frederick, MD 21702, USA.

[5]Laboratory Animal Sciences Program, Leidos Biomedical Research Inc., Frederick National Laboratory for Cancer Research, NIH, Frederick, MD 21701, USA.

[6]Collaborative Protein Technology Resource, National Cancer Institute, NIH, Bethesda, MD 20892, USA.

[7]Systems Biology Center, National Heart Lung and Blood Institute, NIH, Bethesda, MD 20892, USA.

Abstract

The RAS isoforms are frequently mutated in many types of human cancers, including PAX3/PAX7 fusion-negative rhabdomyosarcoma. Pediatric RMS arises from skeletal muscle progenitor cells that have failed to differentiate normally. The role of mutant RAS in this differentiation blockade

[*]Corresponding author. yoheme@mail.nih.gov (M.E.Y.); khanjav@mail.nih.gov (J.K.).

[‡]Present address: Vertex Pharmaceuticals, Boston, MA 02210, USA.

[†]These authors contributed equally to this work.

Author contributions:

M.E.Y. developed the overall concept, performed the experiments, analyzed the data, and wrote the manuscript. B.E.G. helped develop the overall concept, performed the experiments and bioinformatic experiments, analyzed the data, and edited the manuscript. Y.K.S. performed the next-generation sequencing and quantitative reverse transcription PCR experiments. H.-C.C. helped performing the ChIP-seq and DNase-seq bioinformatics experiments. J.F.S and J.S.W. helped develop the overall concept and edited the manuscript. S.S., A.W., and R.P. performed the RNA-seq analysis. X.Z. performed the high-throughput drug screening experiments. A.M., K.A.I., C.M.R, P.A., and S.D. helped design and execute xenograft experiments. D.B. and E.F.E. performed and analyzed the IHC experiments. J.-Q.C. and X.L. performed the Simple Western experiments. R.G. analyzed the high-throughput drug screening data. K.Z., C.J.T., and M.F. helped develop the overall concept. J.K. supervised the overall study, helped develop the overall concept, and edited the manuscript.

Competing interests: The authors declare that they have no competing interests.

Data and materials availability: Raw sequencing data and processed files have been made available through Gene Expression Omnibus SuperSeries accession number GSE85171.

is incompletely understood. We demonstrate that oncogenic RAS, acting through the RAF–MEK [mitogen-activated protein kinase (MAPK) kinase]–ERK (extracellular signal–regulated kinase) MAPK effector pathway, inhibits myogenic differentiation in rhabdomyosarcoma by repressing the expression of the prodifferentiation myogenic transcription factor, MYOG. This repression is mediated by ERK2-dependent promoter-proximal stalling of RNA polymerase II at the *MYOG* locus. Small-molecule screening with a library of mechanistically defined inhibitors showed that RAS-driven RMS is vulnerable to MEK inhibition. MEK inhibition with trametinib leads to the loss of ERK2 at the *MYOG* promoter and releases the transcriptional stalling of *MYOG* expression. MYOG subsequently opens chromatin and establishes super-enhancers at genes required for late myogenic differentiation. Furthermore, trametinib, in combination with an inhibitor of IGF1R, potently decreases rhabdomyosarcoma cell viability and slows tumor growth in xenograft models. Therefore, this combination represents a potential therapeutic for RAS-mutated rhabdomyosarcoma.

INTRODUCTION

More than 30% of all human malignancies, including pancreatic, colorectal and lung cancer, head and neck cancer, melanoma, and hematologic malignancies, are driven by mutant RAS isoforms (1). Despite this knowledge, effective therapies targeting oncogenic mutations in RAS isoforms have yet to be designed. Current attempts to therapeutically target RAS are focused on inhibition of the predominant downstream signaling pathways that are important for maintenance of cell growth and proliferation, such as the RAF–MEK [mitogen-activated protein kinase (MAPK) kinase]–ERK (extracellular signal–regulated kinase) MAPK pathway and the phosphatidylinositol 3-kinase (PI 3-kinase)–AKT–mammalian target of rapamycin (mTOR) pathway (2). Although clinical responses to inhibitors targeting these pathways are frequent, the durability of the response is limited by incomplete apoptosis and the subsequent development of resistance to the targeted agent (3, 4). In addition to its well-characterized roles in malignant transformation and tumor progression, RAS plays a cell type-specific role in cellular differentiation. Expression of oncogenic RAS isoforms inhibits differentiation of neutrophil precursors (5), thyroid epithelial cells (6), and skeletal muscle cells (7). The mechanism by which oncogenic RAS affects differentiation is incompletely understood, but restoration of differentiation represents a potential therapy for RAS-mutated cancers.

PAX3/7 fusion-negative rhabdomyosarcoma (FN-RMS) arises from skeletal muscle precursors that have failed to differentiate normally despite the expression of the myogenic master transcription factor *MYOD1.* The most common somatic mutations in FN-RMS tumors are oncogenic changes in the RAS isoforms (*NRAS, HRAS,* or *KRAS*) at near equivalent frequency (*8, 9*). The distribution of RAS mutations in FN-RMS is unusual because, among the human RAS-driven tumors, only multiple myeloma has a high frequency of mutation of more than one RAS isoform (2). Clonal analysis suggests that RAS mutations occur early in the development of RMS (10), and functional studies confirm that RAS mutation is a driving event. For example, growth of RD (an FN-RMS cell line with an activating mutation in *NRAS*) is dependent on the RAS-RAF-MEK-ERK MAPK signaling pathway (11). Animal models of FN-RMS confirm a central role for aberrant RAS activity

in FN-RMS tumorigenesis (12–19). In addition, a high-throughput small-molecule screen for myogenic differentiating agents in RD identified a MEK inhibitor (20), although the mechanism of the differentiation was not reported. The mechanistic link between aberrant RAS activity and an inability to implement a differentiation program has not previously been described in FN-RMS.

Here, we use a combination of high-throughput drug screening and genome-wide approaches to demonstrate that aberrant MAPK activity both maintains tumor cell proliferation and prevents myogenic differentiation. Suppression of the myogenic differentiation program occurs through transcriptional reprogramming driven by changes in RNA polymerase II (Pol II) activity, chromatin accessibility, histone modifications, and transcription factor deposition. This transcriptional reprogramming is reversed through the action of trametinib (also called GSK1120212), a U.S. Food and Drug Administration–approved, second-generation inhibitor of MEK1/2 (21). We further show that trametinib, in combination with an inhibitor of IGF1R (BMS-754807), suppresses tumor growth in xenograft models of RAS-mutated RMS, providing a strong rationale for the clinical testing of this drug combination in patients with FN-RMS driven by oncogenic RAS.

RESULTS

Oncogenic RAS blocks myoblast differentiation through the MAPK pathway

Constitutively active mutants of *NRAS* and *HRAS* block differentiation in C2C12 mouse myoblasts (7), but the RAS effector pathway responsible for this block has not been elucidated. To determine which pathway is critical for maintenance of the differentiation block, we created stable C2C12 lines expressing constitutively active versions of three RAS effectors: BRAF V600E, myristoylated AKT (Myr-AKT), and RALA Q75L (fig. S1A). Expression of BRAF V600E blocked myogenic differentiation, as evidenced by reduced differentiation and fusion indices in C2C12 myoblasts (Fig. 1A). These results corroborate previous reports in which expression of BRAF, activated by either truncation or constitutive membrane association, in myoblasts prevented terminal differentiation (22–25). Expression of Myr-AKT enhanced C2C12 differentiation, which is consistent with the fact that treatment of myoblasts with inhibitors of AKT or its activator, PI 3-kinase, blocks differentiation (26, 27), whereas loss of PTEN, a negative regulator of PI 3-kinase, increases differentiation and induces skeletal muscle hypertrophy (28). Expression of Myr-AKT also induced myocyte hypertrophy as shown by increased myocyte width. Expression of constitutively active RALA also enhanced C2C12 differentiation (Fig. 1A), in contrast to previous reports in which expression of a RAS mutant that can engage only the RALA activator, RALGDS, prevents myoblast differentiation (29). These results highlight the centrality of the MAPK pathway in the establishment of a myoblast differentiation block.

Oncogenic RAS is necessary for FN-RMS cell survival

As detailed above, mutant RAS is an important oncogenic driver in FN-RMS. Several of the established human FN-RMS cell lines currently in use have oncogenic mutations in one of the RAS isoforms (30). We tested whether expression of oncogenic RAS was necessary for the survival of these cell lines. Stable knockdown of *NRAS* expression in RD, which

expresses *NRAS* Q61H, using short hairpin RNA led to decreased cell viability in a clonogenic assay (fig. S1B). These results are consistent with a previous study that showed the antiproliferative effects of decreased *NRAS* expression in RD using cell titer assays (11). We extended the analysis to show that decreased *NRAS* expression resulted in the induction of cell death by apoptosis, as determined by immunoblot for cleaved poly(adenosine 5′-diphosphate–ribose) polymerase and cleaved caspase-3, in RD. In addition, knockdown of *NRAS* expression decreased levels of phospho-ERK, suggesting that the RAF-MEK-ERK MAPK pathway is activated downstream of mutant NRAS in RD (fig. S1B). Similarly, stable knockdown of *HRAS* expression in SMS-CTR, which expresses *HRAS* Q61K, led to decreased cell viability, induction of apoptosis, and decreased phospho-ERK (fig. S1C). These results confirm the dependency of FN-RMS cell lines on expression of oncogenic *NRAS* and *HRAS.*

MEK inhibitors potently and selectively decrease FN-RMS viability

To identify pathways of vulnerability in FN-RMS in an unbiased manner, we performed a dose-response drug screen for cell viability using a panel of 1912 drugs (31). In this analysis, 12 cell lines were used: 4 PAX3-FP-RMS cell lines, 5 FN-RMS cell lines (4 of which express mutant RAS), and 3 nontransformed cell lines. To identify classes of drugs that selectively inhibited viability of FN-RMS cell lines but not the FP-RMS or nontransformed cell lines, we grouped the compounds by target subcategory and obtained a measure of the in vitro toxicity for each target subcategory in the three categories of cell lines. The potency of a compound was defined by its percent area under the cell viability dose-response curve (%AUC) (table S1 and Fig. 1B). MEK inhibitors ($P = 0.000728$), IGF1R inhibitors ($P = 0.00158$), and topoisomerase I inhibitors ($P = 0.000724$) were selective for RAS-mutated RMS as compared to the nontransformed cell lines. Of these classes of drugs, only the MEK inhibitors were selective for RAS-mutated RMS as compared to FP-RMS ($P = 1.25 \times 10^{-5}$), and therefore, this class was chosen for further study. A summary of the cell viability results for the MEK inhibitors across all the cell lines tested is shown via wind-rose plot in Fig. 1C. The MEK inhibitors as a class were potent in RAS-mutated FN-RMS cell lines, especially BIRCH and SMS-CTR, whereas the RMS559 cell line, which lacks mutant RAS but harbors a fibroblast growth factor receptor 4 mutation (V550L), was insensitive. In addition, MEK inhibitors had minimal potency in FP-RMS or the human fibroblast cell lines. Dose-response curves for each of the MEK1/2 inhibitors included in the screen are shown in fig. S1D.

Trametinib, a specific, non-adenosine 5′-triphosphate competitive allosteric inhibitor of MEK1/2, was the most consistently effective MEK inhibitor in FN-RMS cell lines, with submicromolar median inhibitory concentration (IC_{50}) values in SMS-CTR, BIRCH, and RD but micromolar IC_{50} values in the FP-RMS cell lines (RH30, RH4, and RH5) (fig. S1D). We confirmed this result of the high-throughput screen by showing that trametinib decreased cell viability in RD and SMS-CTR but not in RH30 in a 14-day clonogenic assay (Fig. 1D). Trametinib treatment of FN-RMS cells in vitro inhibited phosphorylation of the MEK targets, ERK1/2 (Fig. 1E); however, this inhibition of phosphorylation is short-lived, with rebound ERK phosphorylation observed in SMS-CTR treated with 100 nM trametinib in as few as 24 hours (fig. S1E).

MEK inhibition induces differentiation in FN-RMS

MEK inhibition with trametinib in melanoma cells is largely cytostatic (2). Cell cycle analysis revealed that, as expected, trametinib treatment induced G1 arrest in RD and SMS-CTR (fig. S2A, top). This growth arrest is associated with an induction of p21 expression, consistent with previous results in RD cells using the MEK inhibitor, UO126 (fig. S2A, bottom) (32). Because MAPK signaling inhibits myoblast differentiation (Fig. 1A), we hypothesized that inhibition of this pathway with trametinib in FN-RMS cells would lead to differentiation of FN-RMS cells. In accordance with this hypothesis, we detected MHC after 48 hours of trametinib treatment in SMS-CTR and RD (Fig. 2A), suggesting differentiation via a myogenic pathway. Trametinib induced differentiation in additional RAS-mutated RMS cell lines (BIRCH and JR1) but not in a RAS-wild type, FP-RMS cell line (RH30), suggesting that this phenomenon is specific to RAS-mutated RMS (fig. S2B).

To define the mechanism by which trametinib induces differentiation in FN-RMS, we used RNA sequencing (RNA-seq) to measure changes in gene expression in SMS-CTR treated with trametinib for 48 hours. Differentially expressed genes are summarized via volcano plot in Fig. 2B and listed in table S2. We performed GSEA to examine the functions of the genes altered by treating FN-RMS with trametinib (Fig. 2C and table S3). The most statistically significant changes in SMS-CTR upon 48 hours of trametinib treatment (nominal P value and FDR q value less than 0.05) were up-regulation of muscle-specific genes (blue, top) and down-regulation of cell cycle genes (green, top). In addition, trametinib induced increased expression of genes with MEF2 consensus binding sites in the promoters (blue, bottom), which consist largely of genes important in skeletal muscle differentiation, and decreased expression of genes with E2F consensus binding sites in the promoters (green, bottom), which consist largely of genes important for cell proliferation (Fig. 2C). Similar changes in gene expression were seen for RD treated with trametinib (fig. S2C and tables S4 and S5). These results suggested that trametinib halted cell cycle progression and induced differentiation in a process analogous to physiologic myogenic differentiation.

To confirm this hypothesis, we used existing RNA-seq data (33) to create a human myogenic differentiation signature (HSMMdiff_UP; table S6). There was up-regulation of this signature in RD and SMS-CTR treated with trametinib for as few as 6 hours, and this effect became more pronounced over time (Fig. 2D). We further confirmed these expression changes at the protein level. For example, expression of the myogenic transcription factors *MYOD* and *MYOG* was induced by trametinib treatment in SMS-CTR and RD at the RNA level [Fig. 2B (blue) and fig. S2C], as well as the protein level (Fig. 2E), after 24 hours of trametinib treatment. RNA and protein expression of *MEF2A* increased in RD and SMS-CTR at the RNA and protein level, but this induction required 48 hours of treatment. *MYC* RNA and protein expression, as well as phosphorylation at S62, which stabilizes the MYC protein in an ERK-dependent manner (34), decreased with trametinib treatment in SMS-CTR (Fig. 2E). MYC mRNA expression did not change with trametinib treatment in RD (fig. S2C), although protein expression decreased (fig. S2D). Thus, MYC, induced and stabilized by aberrant ERK signaling, may play a role in FN-RMS cell proliferation and the maintenance of the differentiation block.

Induction of differentiation by trametinib was not due to an off-target effect of the drug, because siRNA-mediated knockdown of *MEK1* expression decreased cell viability and induced differentiation in RD and SMS-CTR (fig. S2E). The myogenic differentiation signature was also enriched in RD transfected with *MEK1* siRNA (Fig. 2D). Other agents that induce G1 arrest, such as the CDK4/6 inhibitor palbociclib, did not induce differentiation in SMS-CTR (fig. S2F). These results suggest that induction of myogenic differentiation is not solely a result of cell cycle inhibition.

Because a variety of MEK substrates in addition to ERK have recently been identified (35), we evaluated whether trametinib induced myogenic differentiation specifically through the inhibition of ERK. ERK inhibitors were not included in the initial drug screen (table S1). The ERK inhibitors—SCH772984, ulixertinib, and Vx11e—decreased cell viability more potently in SMS-CTR than in RD (fig. S2G). SCH772984, which functions both as a direct ERK1/2 kinase inhibitor and as an inhibitor of ERK phosphorylation by MEK (36), was the most potent of the ERK inhibitors studied, whereas the direct ERK1/2 kinase inhibitors, Vx11e and ulixertinib, were slightly less potent. SCH772984, like trametinib, induced G1 arrest (fig. S2H) and differentiation in RD and SMS-CTR (Fig. 2F). In addition, the myogenic differentiation signature was enriched in SMS-CTR treated with SCH77284 (Fig. 2G and table S2). These data suggest that differentiation in mutant RAS-driven RMS occurs through inhibition of ERK.

MEK inhibition releases ERK2 from myogenic differentiation genes

The fact that ERK2 directly impinges on chromatin to regulate the expression of developmental genes in embryonic stem (ES) cells (37, 38) led us to hypothesize that ERK2 plays a role in maintaining the block in myogenic differentiation. To test this, we first mapped the genome-wide profile of ERK2-chromatin interactions in SMS-CTR using chromatin immunoprecipitation sequencing (ChIP-seq). We identified a total of 3742 ERK2 binding sites ($P < 1 \times 10^{-3}$), 12% of which are promoter-proximal (table S7 and fig. S3A). Functional annotation of the ERK2 targets using Genomic Regions Enrichment of Annotations Tool (GREAT) ontology (39) revealed a strong association with muscle-specific processes and differentiation (Fig. 3A, top). This association appears to be cell type–dependent because, in SK-N-AS, a neuroblastoma cell line with mutant *NRAS* (Q61K), there was a strong association with neural crest cell–specific genes (fig. S3B, top). Motif analysis of the ERK2-bound loci identified enriched motifs for known myogenic transcription factors including MYF5, MYOD, and MYOG, as well as known substrates of MAPK signaling including the AP-1 family of transcription factors (FOSL1, FOSL2, and JUN) (Fig. 3A, bottom). Enrichment for AP-1, but not myogenic, transcription factor motifs was maintained in SK-N-AS (fig. S3B, bottom), again indicating that ERK2-bound loci are lineage-specific.

We also performed ERK2 ChIP-seq analysis on SMS-CTR treated with trametinib. The ERK2 signal intensity decreased by at least two-fold at about 50% of ERK-binding sites with trametinib treatment ($P = 2.8 \times 10^{-53}$, paired *t* test; Fig. 3B). For a subset of genes ($n = 25$), trametinib treatment resulted in both decreased ERK2 deposition in the promoter and increased gene expression [at least twofold increase in fragments per kilobase of transcript

per million mapped reads (FPKM); table S7]. For these genes, the significantly enriched gene ontology terms “sarcomere,” “myofibril,” and “contractile fiber” [DAVID (Database for Annotation, Visualization, and Integrated Discovery) (40); $P < 0.05$, Bonferroni correction applied) are consistent with these genes being important for myogenesis. Examples of genes for which trametinib decreased promoter ERK deposition and increased gene expression include the myogenic transcription factor *MYOG* (Fig. 3B, right).

In mouse ES cells, developmental genes are held in a poised state to facilitate rapid induction of gene expression. The poised state is marked by the presence of histone modifications associated with both transcriptional activation (for example, H3K27ac) and transcriptional repression (for example, H3K27me3), as well as a poised form of RNA Pol II that is phosphorylated on S5 of the C-terminal domain repeats by ERK2 (38). During normal differentiation, H3K27me3 is removed, and S2 residues in the C-terminal domain are phosphorylated by P-TEFb, thus marking these genes as active and allowing transcriptional elongation. To test the hypothesis that *MYOG* expression is regulated in this way in FN-RMS, we first performed ChIP-seq experiments for H3K27me3 and H3K27ac in the presence and absence of trametinib. Substantial deposition of H3K27ac but not of H3K27me3 was observed at the *MYOG* locus (Fig. 3C, left), in contrast to the *FBXO32* locus, which is known to be repressed in a PRC2-dependent manner in RMS (41), which shows deposition of H3K27me3 but not of H3K27ac (Fig. 3C, right). Deposition of H3K27ac and H3K27me3 at the *MYOG* locus was unchanged by trametinib treatment despite the increase in the gene’s expression (Figs. 3D and 2E) and loss of ERK2 deposition (also shown by ChIP-qPCR in Fig. 3E). This result was unexpected given that H3K27ac deposition did increase at the *MYOG* locus during the transition from normal skeletal muscle myoblasts to myotubes (fig. S3C).

We then tested the hypothesis that ERK-dependent phosphorylation of RNA Pol II is responsible for repression of *MYOG* expression in FN-RMS by performing ChIP-seq experiments for total RNA Pol II, as well as for RNA Pol II phosphorylated at S2 and S5 residues in the C-terminal domain. RNA Pol II accumulated in the promoterproximal region of *MYOG* (Fig. 3F) in control cells rather than the transcriptional start site region (TSSR; fig. S3D). Upon trametinib treatment, RNA Pol II signal was decreased in the promoter-proximal region and increased both in the TSSR and throughout the body of the gene (Fig. 3F), causing little change in pausing index (42). This indicates that RNA Pol II promoter stalling (failed TSS entry) rather than pausing was associated with suppression of *MYOG* transcription (fig. S3, D to E). S5-phosphorylated RNA Pol II also accumulated in the promoter-proximal region of *MYOG* in control cells, but this deposition of S5-phosphorylated RNA Pol II decreased in the presence of trametinib. In contrast, S2-phosphorylated RNA Pol II was almost absent in the control cells, indicating very little transcriptional elongation, but was detected in the region downstream of the poly-adenylation signal in trametinib-treated cells, indicating active transcriptional elongation (Fig. 3F). These data suggest that, in RAS-mutated RMS, ERK2 represses *MYOG* expression through promoter-proximal binding leading to S5-phosphorylation and stalling of RNA Pol II. Consistent with this, selective inhibition of the RNA polymerase C-terminal domain kinases CDK7 (THZ1) and CDK9 (flavopiridol) blocks the trametinib-dependent induction of *MYOG* expression in SMS-CTR (fig. S3F).

To confirm that ERK2 deposition at the *MYOG* promoter is a function of signaling downstream of mutant RAS, we overexpressed oncogenic forms of *HRAS, KRAS,* and *NRAS* in C2C12 mouse myoblasts (fig. S3G). As expected, the C2C12 cells overexpressing oncogenic RAS failed to differentiate under serum-starved conditions (fig. S3H), whereas vector control cells readily differentiated. ERK2 deposition was increased at the *MYOG* promoter in C2C12 cells overexpressing oncogenic RAS (Fig. 3G, left). In RAS–wild-type C2C12 cells, serum starvation resulted in loss of ERK2 at the *MYOG* promoter (Fig. 3G, right), analogous to MEK inhibition in FN-RMS. These data support the hypothesis that ERK2 plays a role in suppressing myogenic differentiation by directly impinging on the *MYOG* promoter, both in FN-RMS and in normal myoblasts.

MEK inhibition induces changes in chromatin accessibility in RAS-mutated RMS

Our data support a model whereby, in RAS-mutated FN-RMS, ERK2 phosphorylates and stalls RNA Pol II at the *MYOG* promoter, preventing expression despite an active chromatin state. With the continuous MAPK signaling that results from the oncogenic RAS mutation, ERK2 remains at this site, preventing RNA Pol II TSS loading and elongation on the *MYOG* gene. In the presence of the MEK inhibitor, trametinib, ERK2 is no longer localized at the *MYOG* promoter, leading to promoter release of RNA Pol II, allowing complete transcription of *MYOG.* During normal muscle development, expression of *MYOG* triggers the expression of myotube-specific genes (43). Therefore, we hypothesized that *MYOG* induction in FN-RMS would similarly induce expression of myotube-specific genes. Consistent with this idea, we observed that overexpression of *MYOG* in RD cells did induce phenotypic differentiation (fig. S4A).

To further interrogate whether induction of these differentiation genes was driven by alterations in chromatin accessibility, we compared the changes in chromatin accessibility, as defined by deoxyribonuclease (DNase) hypersensitivity, between DMSO- and trametinib-treated SMS-CTR (fig. S4B). Regions for which alterations in DNase hyper-sensitivity peak intensity were consistent across two biological replicates were identified as increased accessibility (n = 9779), unchanged, or decreased accessibility (n = 8569) (table S8). Motif analysis showed that the basic helix-loop-helix (bHLH) transcription factor motifs were strongly enriched in the regions in which chromatin accessibility is increased because of trametinib treatment. Basic leucine zipper (bZIP) motifs, such as those for the AP-1 transcription factors whose expression is increased by active ERK, were enriched in the decreased accessibility regions (Fig. 4A). Gene ontology analysis showed that the increased accessibility regions were enriched in genes important for skeletal muscle development, whereas decreased accessibility regions were enriched in ERK-induced negative regulators of the MAPK pathway (Fig. 4B) (44). Genome-wide assessment of MYOG occupancy was also performed by ChIP-seq analysis. We identified very few MYOG peaks in control cells, consistent with the low *MYOG* expression in these cells (n = 782); however, the number of MYOG peaks markedly increased in the presence of trametinib (n = 9337, fig. S4C). MYOG deposition increased in the increased accessibility regions, but MYOG was largely absent in the decreased accessibility regions (Fig. 4C).

The related bHLH transcription factors, *MYC* and *MYOD,* play antagonizing roles in the induction of normal myogenic differentiation (45, 46). The roles that these transcription factors play in trametinib-induced differentiation of FN-RMS were assessed with ChIP-seq experiments, which identified 19,135 MYOD peaks and 3383 MYC peaks in vehicle (DMSO)–treated SMS-CTR cells (table S9). In addition, patterns of key histone marks and CTCF were used to define chromatin states with ChromHMM (47). This analysis determined that, although MYC associates primarily with active promoters in FN-RMS, consistent with its role in other cancers as a general transcriptional amplifier (48), MYOD was predominantly localized in chromatin regions enriched with the histone modifications associated with strong enhancers (Fig. 4D), especially H3K27ac and H3K4me1/2.

In studies of differentiating murine and human skeletal muscle myoblasts, most MYOD-binding regions are shared in both the myoblast and myotube state (*49, 50*). Here, MYOD deposition correlated with DNase hypersensitivity, with increasing MYOD deposition in regions that increased in chromatin accessibility as a function of trametinib treatment (Fig. 4C). In contrast, MYC did not accumulate in the increased accessibility regions, consistent with the decrease in MYC expression due to trametinib treatment (Figs. 4C and 2E). However, for MYOD, about 40% of the binding regions were shared in the presence and absence of trametinib, whereas an additional subset of MYOD-bound regions was identified exclusively in cells treated with trametinib (fig. S4C). In addition, many genomic sites with increased chromatin accessibility as a function of trametinib treatment are co-occupied by MYOD and MYOG (Fig. 4E), suggesting that MYOG acts as a master transcription factor and facilitates the opening of chromatin regions and recruitment of MYOD.

DNase hypersensitivity peaks were linked to their nearest gene within topologically associated domain boundaries as previously described (51) to compare trametinib-induced changes in gene expression as a function of chromatin state (Fig. 4F). This analysis showed that the expression of genes near decreased accessibility regions decreased significantly ($P < 0.0001$), and expression of genes near increased accessibility regions increased significantly ($P < 0.0001$) when compared to genes near unchanged accessibility regions. Among the increased accessibility regions, the expression of genes near regions of accessible DNA that overlap with at least one MYOG peak was higher than regions lacking MYOG (Fig. 4F, right). The large majority (90%) of trametinib-induced MYOG peaks occurred at enhancers, and the deposition of H3K27ac increased at these sites with trametinib treatment, indicating that MYOG might play a role in establishing new enhancers (fig. S4D, left). However, there was no increase in H3K27ac at the promoters in which trametinib induced MYOG deposition (fig. S4D, right).

MEK inhibition remodels the super-enhancer landscape in RAS-mutated FN-RMS

Because super-enhancers are often defined by their disproportionately large H3K27ac load, we asked whether the changes in H3K27ac deposition with trametinib treatment in SMS-CTR also changed which genes were associated with super-enhancers. We first identified 571 super-enhancers in SMS-CTR (Fig. 5A, top, and table S10). Because cancer cell lines frequently exhibit differences in enhancer signatures from their corresponding primary tumors (52, 53), we identified super-enhancers in 40 additional samples, including FN-RMS

cell lines and tumors, as well as normal skeletal muscle and other cancer cell lines. A clustering analysis of Pearson's correlations of the H3K27ac signal intensity at the identified super-enhancers across these samples showed that SMS-CTR and other FN-RMS cell lines and tumors form a distinct cluster (fig. S5). These results indicate that super-enhancers are conserved among FN-RMS cell lines and tumors and that the super-enhancers in SMS-CTR are representative of FN-RMS.

To investigate how the super-enhancer landscape in RAS-mutated RMS is changed by MEK inhibition, we identified super-enhancers in trametinib-treated SMS-CTR (577 total). Comparison of the super-enhancer landscape in control and trametinib-treated cells revealed three classes of super-enhancers: those that are unchanged with trametinib treatment, RAS-dependent super-enhancers that are lost with trametinib treatment, and myogenic super-enhancers that are gained with trametinib treatment (Fig. 5A). Super-enhancers that are unchanged with trametinib treatment occur at loci for genes known to be highly expressed in RMS compared to normal skeletal muscle, including *IGF2, MEST, MYOG,* and *MYOD* (51).

The super-enhancers lost with trametinib treatment occur at loci known to be transcriptionally regulated by active ERK (54), including *SPRY1,* a negative regulator of the MAPK pathway, and *MYC* (Fig. 5B, top, and fig. S6A). Expression of both *MYC* (Fig. 2E and fig. S2E) and Sprouty1, the protein product of *SPRY1* (fig. S6B), decreased with trametinib treatment, corresponding with the loss of their super-enhancers. Using ENCODE (Encyclopedia of DNA Elements) consortium data, we identified super-enhancers in human skeletal muscle myoblasts and myotubes (fig. S6C) (55). Although super-enhancers at *IGF2* and *MEST* were observed in this system, super-enhancers were not observed at *SPRY1* or *MYC* in these cells, indicating that the presence of these super-enhancers in SMS-CTR was due to oncogenic RAS. We used publicly available data to show that super-enhancers at loci encoding negative regulators of MAPK signaling, such as *SPRY4,* are observed in other RAS-mutated RMS cell lines and tumors but not in RAS-wild-type FN-RMS tumors or normal skeletal muscle. The *SPRY4* super-enhancer was also seen in RAS-mutated cell lines derived from other human cancers, including hepatocellular carcinoma and colorectal carcinoma (fig. S6D).

The super-enhancers gained with trametinib treatment, such as those seen at the *MYH3* locus (Fig. 5B, bottom), occur at genes expressed late in the process of myogenic differentiation (49). Super-enhancers were also gained at these loci in differentiating myotubes (fig. S6C). The super-enhancer at the *MYOG* locus was unchanged by trametinib ($P = 0.894$; Fig. 5A), consistent with the change in *MYOG* expression being driven by release of stalled RNA Pol II and not by alterations in histone acetylation or chromatin accessibility. The number of MYOG peaks per enhancer was highest in super-enhancers in trametinib-treated cells (Fig. 5C), suggesting that MYOG deposition assists in establishment of super-enhancers at genes important for myogenic differentiation. On a genome-wide scale, the expression of genes linked to RAS-dependent super-enhancers decreased with trametinib treatment, whereas the expression of genes linked to myogenic super-enhancers increased with trametinib treatment (Fig. 5D). We infer that the expression of mutant RAS in SMS-CTR locked the super-enhancer landscape in this myoblast-like cell type, which is

effectively reversed by MEK inhibition. The expression of master transcription factors is frequently regulated by super-enhancers, and, in turn, the motifs for each cell type's master transcription factors are commonly found in that cell's super-enhancers (53). Assessment of the circuitry of super-enhancer-regulated transcription factors in control- and trametinib-treated SMS-CTR showed that MYOG is a central transcription factor in trametinib-treated cells (Fig. 5E), which is consistent with MYOG's association with regions of chromatin that increase in accessibility upon trametinib treatment (Fig. 4). MEK inhibition in RAS-mutated RMS thus induces expression of *MYOG,* a master transcription factor, which in turn establishes super-enhancers at myogenic loci.

MEK inhibition impairs tumor growth, induces differentiation, and prolongs murine survival in xenograft models of RAS-mutated RMS

Differentiation therapy is used effectively in the treatment of both acute promyelocytic leukemia and high-risk neuroblastoma (56) and is a promising approach for FN-RMS. To determine whether MEK inhibition might represent a strategy for differentiation therapy in RAS-mutated RMS, the effects of trametinib on in vivo tumor growth were studied. Orthotopic xenograft models of RAS-mutated RMS were made by injecting SMS-CTR, BIRCH, or RD into the gastrocnemius muscle of immunodeficient mice. Palpable tumors developed with each of the cell lines tested with an average latency of 3 weeks. Trametinib treatment inhibited tumor development and led to a significant survival advantage in SMS-CTR ($P = 0.014$) and BIRCH models ($P = 0.0067$; Fig. 6A) but had modest effects in the RD model (fig. S7, A and B). However, progressive disease was ultimately noted in all the RAS-mutated RMS xenografts treated with trametinib (Fig. 6A and fig. S7A). No weight loss was observed in the trametinib-treated mice (fig. S7C). Trametinib treatment decreased ERK phosphorylation by 70% within SMS-CTR tumors but by only 50% in BIRCH (Fig. 6B) and RD tumors (fig. S7D), as determined by a quantitative capillary immunoassay. Trametinib treatment also increased *MYOG* expression within the tumors, as determined by both immunoblot of tumor lysates (Fig. 6C and fig. S7E) and immunohistochemistry (IHC) of formaldehyde-fixed tumors (Fig. 6D and fig. S7F), suggesting that MEK inhibition initiated differentiation of RAS-mutated RMS in vivo. Consistent with our model, at the RNA level, there was an up-regulation of genes associated with myogenically induced super-enhancers, and concomitant down-regulation of RAS-dependent super-enhancer genes (table S16), in trametinib-treated SMS-CTR tumors (Fig. 6E). However, complete phenotypic terminal differentiation was not observed in these tumor models.

Dual blockade of IGF1R and the RAS-MEK-ERK MAPK pathway synergistically inhibits FN-RMS growth in vitro and in vivo

Because progressive disease was ultimately noted in all the RAS-mutated RMS xenografts treated with trametinib, we hypothesized that a combination of pathway inhibitors would be needed to achieve durable remissions. To identify active combinations of drugs, an in vitro combination matrix screen was performed. The most potent 35 compounds from the single-agent drug screen (table S1), which included trametinib, were combined in a pairwise, all-versus-all fashion in 6 × 6 dose-response matrices on a high-throughput screening platform, resulting in 595 individual matrices. The drug/drug combinations were ranked using the excess over the highest single-agent (HSA) method. The highest scoring combination across

three RAS-mutated cell lines was trametinib plus GSK-2126458, a dual PI 3-kinase/mTOR inhibitor, and other high scoring combinations included trametinib plus other inhibitors of the PI 3-kinase/mTOR/AKT pathway (table S17). Combining a MEK inhibitor and a PI 3-kinase inhibitor has been previously tested in RMS (57), but the therapeutic benefit of these combinations has been limited in clinical trials because of toxicity. On the basis of these pilot results, we performed a 10 × 10 dose-response validation matrices using an expanded set of PI 3-kinase/mTOR/AKT/MEK/ERK inhibitors. This included 25 highly active agents in 96 discrete matrices (table S18). The highest scoring combination in both RD and SMS-CTR was trametinib plus BMS-754807, a small-molecule inhibitor of IGF1R (Fig. 7, A and B, and table S18). This combination was also highly synergistic in another HRAS-driven cell line, BIRCH. In addition to its effects on cell proliferation, the combination of trametinib and BMS-754807 induced caspase-3/7 activity (Fig. 7C) and cell surface translocation of phosphatidylserine, as detected by annexin V staining (Fig. 7D), in SMS-CTR, consistent with induction of apoptosis. These results suggest that there may be therapeutic benefit to combining a MEK inhibitor, such as trametinib, with an IGF1R inhibitor, such as BMS-754807, in RAS-driven RMS. Simultaneous targeting of MEK and IGF1R has induced tumor regression in RAS-driven acute leukemia, colorectal carcinoma, and non–small cell lung cancer models but has yet to be tested in clinical trials (58–61).

In the basal state, ERK initiates a negative feedback loop by inducing expression of members of the dual-specificity phosphatase (DUSP) and sprouty (SPRY) families, which we show above to have RAS-dependent super-enhancers (Fig. 5). Induction of DUSPs and SPRYs leads to decreased phosphorylation of receptor tyrosine kinases, such as IGF1R, and intracellular kinases, such as RAF and MEK. In the presence of MEK inhibition, this negative regulation is lost (62). We hypothesized that trametinib treatment would induce phosphorylation of IGF1R in RAS-driven RMS through loss of this negative regulation. We used a quantitative capillary immunoassay to confirm the results shown in fig S1E that short-term trametinib treatment (6 hours) abrogated ERK phosphorylation but that rebound ERK phosphorylation occurred with longer treatment (48 hours). In addition, AKT phosphorylation increased with trametinib treatment (Fig. 7, E and F). Finally, trametinib treatment induced IGF1R phosphorylation (Fig. 7, E and F). We further hypothesized that treatment with trametinib and the IGF1R inhibitor, BMS-754807, would prevent the phosphorylation and activation of IGF1R induced by trametinib treatment alone. Consistent with this idea, BMS-754807 treatment alone blocked the basal phosphorylation of IGF1R induced by growing cells in full serum, and the addition of BMS-754807 to trametinib prevented the phosphorylation of ERK, AKT, and IGF1R induced by treatment with trametinib alone (Fig 7F). IGF1R inhibition therefore synergizes with MEK inhibition in RAS-driven RMS by augmenting inhibition of ERK phosphorylation and inhibiting AKT phosphorylation.

To test whether the observed in vitro synergy between trametinib and BMS-754807 would correspond to therapeutic enhancement for the combination in vivo, we evaluated the SMS-CTR (Fig. 7G) and RD (fig. S8A) xenograft models. We observed a prolonged tumor growth delay for mice treated with the combination versus either single agent. In SMS-CTR, tumor growth in the combination mice began 40 days after treatment had stopped (four tumor doubling times). In addition, for SMS-CTR, the observed tumor growth delay was associated

with significant prolongation of overall survival for the mice treated with the combination compared to trametinib ($P < 0.0001$) or BMS-754807 alone ($P < 0.0001$; Fig 7H), whereas, for RD, a survival advantage was not observed for the combination (fig. S8B). In addition to causing a tumor growth delay, treatment with the combination oftrametinib and BMS-754807 induced tumor regression in SMS-CTR (Fig. 7I) and stabilized growth of RD tumors (fig S8C). Toxicity was observed in the combination group; one mouse treated with the combination in the RD model was euthanized because of excessive body weight loss early in the study, and the combination-treated mice had the lowest body weight throughout the treatment course, which recovered when the treatment was stopped (fig. S8D). Phosphorylation of ERK and AKT, as well as expression of IGF1R, was decreased in tumor lysates from SMS-CTR xenografts treated with trametinib and BMS-754807, indicating that the in vitro mechanism of synergy between these two drugs was preserved in vivo (fig. S8E). These results suggest that addition of an IGF1R inhibitor to a MEK inhibitor provided therapeutic enhancement in RAS-mutated RMS.

DISCUSSION

We elucidated an epigenetic mechanism by which MEK inhibition induces differentiation in FN-RMS. Our data support a model in which oncogenic RAS, signaling through the MAPK pathway, drives FN-RMS cell proliferation and inhibits the expression of *MYOG,* which prevents initiation of myogenic differentiation (fig. S9, left). This differentiation block is created by an interaction between ERK2 and RNA Pol II at the *MYOG* locus, which stalls transcription of *MYOG.* However, in the presence of trametinib, ERK-dependent inhibition of *MYOG* expression is released, and ERK-mediated activation of *MYC* and of AP-1–dependent cell proliferation is inhibited (fig. S9, right). MYOG subsequently binds additional skeletal muscle–specific loci and induces H3K27 acetylation, chromatin opening, and, ultimately, gene transcription at those loci.

Using FN-RMS as a model system, we show that MEK inhibition dramatically affects the super-enhancer landscape. The impact of RAS on the super-enhancer landscape has been previously studied in mouse embryonic fibroblasts engineered to express HRAS G12V (63) but not in patient-derived cancer cell lines. Cancer cells are known to acquire super-enhancers at the loci of known oncogenes (64). In the case of FN-RMS, we have identified super-enhancers at the loci for *SPRY1* and *SPRY4,* as well as the known oncogene, *MYC*. These super-enhancers were not identified in normal human myoblasts, indicating that they are acquired during tumorigenesis. Furthermore, they are observed in other RAS-mutated cell lines. Therefore, RAS-driven transformation may induce de novo establishment of super-enhancers at loci encoding oncogenes.

Normal skeletal muscle differentiation is initiated by the coordinated action of master transcription factors, including MYOD and MYOG. MYOD activates the expression of MYOG, which interacts with the MEF2 family transcription factors to drive terminal differentiation (43). The role of the RAF-MEK-ERK MAPK pathway in this process is controversial, with evidence that this pathway has different roles in the early and later stages of differentiation. MEK and ERK inhibit the ability of MYOD to induce MYOG expression (*65, 66*), an early differentiation event, by binding and phosphorylating MYOD, respectively

(67). Here, we show that nuclear ERK2 also inhibits MYOD function by binding chromatin and preventing MYOG expression, which is supported by the fact that blocking nuclear translocation of ERK2 induces early myogenic differentiation (68). However, genetic knockdown of ERK2 expression in myoblasts prevents fusion of myoblasts into multinucleated myotubes (69), and mice lacking ERK1/2 selectively in skeletal muscle fibers have muscle fiber atrophy and loss (70), suggesting a critical role for MEK-ERK signaling in the later stages of myogenic differentiation.

The efficacy of MEK inhibitors in FN-RMS has been investigated previously, with conflicting results. Initial studies using the MEK inhibitor tool compound, UO126, showed efficacy in the RD cell line in vitro and in xenograft models (71, 72). In addition, the RD cell line was sensitive to the first-generation MEK inhibitors in vitro (11, 73), but treatment of RD xenografts with one such MEK inhibitor, selumetinib, did not result in tumor growth delay in vivo (57). An in vitro screen of a panel of compounds in RD and several patient-derived tumor cell lines failed to highlight MEK inhibitors as potent inhibitors of cell viability (8). However, a sarcoma cell line screen of oncology drugs showed that the FN-RMS cell lines RD and RH36 (also known as BIRCH) (30) were sensitive to MEK inhibitors, but the dose-response curves lacked the typical sigmoidal shape (74). We also observe an atypical shape in the dose-response curve for trametinib in RD. This curve shape is likely due to the cytostatic response to trametinib in this cell line.

In our study, trametinib monotherapy was more effective in treating xenografts of *HRAS*-mutated cell lines (SMS-CTR and BIRCH) than xenografts of the *NRAS*-mutated cell line, RD. MEK inhibitors had not been tested in these *HRAS*-mutated xenografts before this study. Several potential explanations exist for the differential sensitivity of *HRAS*- and *NRAS*-mutated FN-RMS cell lines to MEK inhibition. There are cooperative mutations in addition to the RAS mutations in these cell lines that could affect MEK inhibitor sensitivity and drive tumorigenesis. For example, because of uniparental disomy at the 11p15.5 locus, SMS-CTR and BIRCH express only mutant *HRAS.* Increased gene dosage of mutant *NRAS* increases sensitivity to MEK inhibition (75); increased gene dosage of mutant *HRAS* could function similarly. RD also has a loss-of-function mutation in the RAS guanosine triphosphatase–activating protein, *NF1* (E977X), which could contribute to the resistance of this cell line to chemotherapeutics and targeted agents. Alternatively, the differential response between *HRAS*- and *NRAS*-mutated FN-RMS cell lines to trametinib could be due to RAS isoform–specific differences in engagement of effector pathways.

There are several limitations associated with this study. First, although we show that transcription of *MYOG* is released by MEK inhibition, the mechanism by which ERK2 stalls *MYOG* transcription has not been fully elucidated. Second, although MEK inhibition induces terminal differentiation in RAS-mutated RMS cells in vitro, in tumors, MEK inhibition up-regulated a subset of downstream myogenic super-enhancer–associated genes but not a key marker of complete muscle differentiation, *MYH3.* Whether this lack of terminal differentiation in vivo is due to a technical issue or the incomplete elimination of intra-tumoral ERK phosphorylation will be addressed by future experiments.

In summary, we used an unbiased, high-throughput drug screen to identify the MAPK pathway as a key vulnerability in RAS-mutated RMS. Using phenotypic and transcriptomic approaches, we showed that MEK inhibition induced a skeletal muscle differentiation program in RAS-mutated RMS cells. We demonstrated that RAS-mutated RMS is locked in a myoblast-like state through ERK2 deposition at the *MYOG* promoter, which stalls *MYOG* transcription. MEK inhibition with trametinib allowed *MYOG* expression and enabled *MYOG* to induce the differentiation program. The vulnerability of RAS-mutated RMS to MEK inhibition observed in cell culture models was confirmed in xenograft experiments where trametinib both inhibited tumor growth and induced differentiation. The in vivo tumor growth suppression observed with trametinib monotherapy was incomplete, but combining trametinib with the IGF1R inhibitor, BMS-754807, achieved remissions in xenograft models of RAS-mutated RMS and represents a meaningful opportunity for clinical translation.

MATERIALS AND METHODS

Study design

This study was designed to identify drugs that would specifically inhibit the growth of RAS-mutated RMS cells in culture and in xenograft models. Using the MIPE-v4 library of mechanistically characterized drugs, we identified that MEK inhibitors in general and trametinib selectively inhibited growth of RAS-mutated RMS cells as compared to cells derived from the related childhood sarcoma, PAX FP-RMS. The mechanism by which trametinib inhibits RAS-mutated RMS cell growth was assessed using a combination of cell cycle analysis, myogenic differentiation, whole-transcriptome sequencing, and immunoblot experiments, which confirmed that trametinib induces myogenic differentiation in RAS-mutated RMS. To better understand how MEK inhibition induced differentiation in RMS cells, we performed various ChIP-seq and ChIP-qPCR experiments in RAS-mutated RMS cells, as well as C2C12 mouse myoblasts expressing mutant RAS isoforms. The efficacy of trametinib in three xenograft models of RAS-mutated RMS was then assessed. In each experiment, mice were randomly assigned to the treatment groups, and mice ($n > 4$) per group were included to achieve statistical significance. Trametinib (3 mg/kg) was administered daily by oral gavage after the establishment of palpable xenografted tumors. Tumor size was measured twice a week with digital calipers, and animals were euthanized when they reached tumor end point (tumor of >2 cm in any dimension). No animals were excluded from analysis. Matrix screening experiments were performed to identify combinations of targeted agents that would improve outcomes in xenograft models of RAS-mutated RMS as compared to trametinib alone. The combination of trametinib and BMS-754807, an inhibitor of IGF1R, was identified as synergistically active in vitro. The efficacy of the combination was then assessed in xenograft models. In this case, mice were randomly assigned to the treatment groups, with $n = 10$ mice per group.

Clonogenic assay

RD, SMS-CTR, or RH30 cells were plated at a density of 100 cells per well in six-well tissue culture plates. The plates were incubated for 2 weeks before fixing in 10% formaldehyde and staining with 0.01% crystal violet.

Differentiation assay

C2C12 cells were serum-starved in Dulbecco's modified Eagle's medium with 2% horse serum (Gibco) for 5 days before immunofluorescence analysis. Differentiation index was calculated as the number of nuclei within an MHC-expressing cell divided by the total number of nuclei in a field. Fusion index was calculated as the number of nuclei within an MHC-expressing cell with greater than two nuclei divided by the total number of nuclei in a field. For the differentiation and fusion indices, a total of three independent fields were quantified. To determine myotube width, the widest portion of 10 individual myotubes per condition was determined.

High-throughput cell viability assays

For each cell line tested, a total of 1000 cells per well in 5 μl of complete RPMI 1640 medium were dispensed into 1536-well white tissue culture plates that had been preplated with the compounds comprising the MIPE-v4 library as previously described (76). Cells were grown in the presence of compounds for 48 hours before addition of a CellTiter-Glo luminescent cell viability assay reagent. Resultant luminescent signal was measured on a ViewLux instrument. AUC from the resultant dose-response curves was calculated using a standard trapezoidal method (31).

Immunofluorescence experiments

Cells were grown in Nunc chamber slides (Lab-Tek), fixed with 4% paraformaldehyde, and permeabilized in 0.5% Triton X-100. Antibodies were diluted in BlockAid (Life Technologies) or 1% bovine serum albumin in phosphate-buffered saline. Coverslips were mounted with ProLong Gold with 4′,6-diamidino-2-phenylindole (Life Technologies) before visualization using an EVOS FL microscope (Life Technologies).

Annexin V assay

SMS-CTR cells were treated with vehicle (DMSO), 100 nM trametinib, 350 nM BMS-754807, or the combination of trametinib and BMS-754807 for 72 hours before harvesting and incubating with allophycocyanin-labeled human recombinant annexin V (BioLegend) and Sytox Green (Thermo Fisher Scientific) according to the manufacturers' instructions. Samples were read on a FACSCanto flow cytometer (BD Biosciences), and percentage of annexin positive cells was calculated in FlowJo.

Statistical analysis

All data are presented as the mean and SEM from at least three independent experiments. Differences between groups were evaluated using paired Student's *t* test after normal distribution was confirmed using the Shapiro-Wilk test, with Welch's correction applied where indicated to account for unequal variances. For mouse survival curve analysis, the median survival from the different groups is presented, and the log-rank (Mantel-Cox) test was used to evaluate differences between the groups. Additional experimental details are available in the Supplementary Materials.

Supplementary Material

Refer to Web version on PubMed Central for supplementary material.

Acknowledgments:

We are grateful to R. Robey, C. Thiele, R. Hawley, B. Stanton, J. Madigan, M. Hall, P. Randazzo, R. Kaplan, V. Sartorelli, J. Waterfall, D. Singer, and D. Levens for helpful discussions and review of the manuscript. The content of this publication does not necessarily reflect the views or policies of the Department of Health and Human Services, nor does mention of trade names, commercial products, or organizations imply endorsement by the U.S. Government. Animal care was provided in accordance with the procedures outlined in the *Guide for the Care and Use of Laboratory Animals* (National Research Council, 2011; National Academies Press). **Funding:** This project has been funded in whole or in part with Federal funds from the National Cancer Institute, NIH, under contract no. HHSN261200800001E. M.E.Y. is funded by an Alex's Lemonade Stand Foundation Young Investigator Award.

REFERENCES AND NOTES

1. Prior IA, Lewis PD, Mattos C, A comprehensive survey of Ras mutations in cancer. Cancer Res 72, 2457–2467 (2012). [PubMed: 22589270]
2. Cox AD, Fesik SW, Kimmelman AC, Luo J, Der CJ, Drugging the undruggable RAS: Mission possible? Nat. Rev. Drug Discov 13, 828–851 (2014). [PubMed: 25323927]
3. Sos ML, Fischer S, Ullrich R, Peifer M, Heuckmann JM, Koker M, Heynck S, Stückrath I, Weiss J, Fischer F, Michel K, Goel A, Regales L, Politi KA, Perera S, Getlik M, Heukamp LC, Ansén S, Zander T, Beroukhim R, Kashkar H, Shokat KM, Sellers WR, Rauh D, Orr C, Hoeflich KP, Friedman L, Wong K-K, Pao W, Thomas RK, Identifying genotype-dependent efficacy of single and combined PI3K- and MAPK-pathway inhibition in cancer. Proc. Natl. Acad. Sci. U.S.A 106, 18351–18356 (2009). [PubMed: 19805051]
4. Villanueva J, Infante JR, Krepler C, Reyes-Uribe P, Samanta M, Chen H-Y, Li B, Swoboda RK, Wilson M, Vultur A, Fukunaba-Kalabis M, Wubbenhorst B, Chen TY, Liu Q, Sproesser K, DeMarini DJ, Gilmer TM, Martin A-M, Marmorstein R, Schultz DC, Speicher DW, Karakousis GC, Xu W, Amaravadi RK, Xu X, Schuchter LM, Herlyn M, Nathanson KL, Concurrent MEK2 mutation and BRAF amplification confer resistance to BRAF and MEK inhibitors in melanoma. Cell Rep 4, 1090–1099 (2013). [PubMed: 24055054]
5. Darley RL, Burnett AK, Mutant RAS inhibits neutrophil but not macrophage differentiation and allows continued growth of neutrophil precursors. Exp. Hematol 27, 1599–1608 (1999). [PubMed: 10560907]
6. De Vita G, Bauer L, Correa da Costa VM, De Felice M, Baratta MG, De Menna M, Di Lauro R, Dose-dependent inhibition of thyroid differentiation by RAS oncogenes. Mol. Endocrinol 19, 76–89 (2005). [PubMed: 15388794]
7. Olson EN, Spizz G, Tainsky MA, The oncogenic forms of N-ras or H-ras prevent skeletal myoblast differentiation. Mol. Cell. Biol 7, 2104–2111 (1987). [PubMed: 3600660]
8. Chen X, Stewart E, Shelat AA, Qu C, Bahrami A, Hatley M, Wu G, Bradley C, McEvoy J, Pappo A, Spunt S, Valentine MB, Valentine V, Krafcik F, Lang WH, Wierdl M, Tsurkan L, Tolleman V, Federico SM, Morton C, Lu C, Ding L, Easton J, Rusch M, Nagahawatte P, Wang J, Parker M, Wei L, Hedlund E, Finkelstein D, Edmonson M, Shurtleff S, Boggs K, Mulder H, Yergeau D, Skapek S, Hawkins DS, Ramirez N, Potter PM, Sandoval JA, Davidoff AM, Mardis ER, Wilson RK, Zhang J, Downing JR, Dyer MA; St. Jude Children's Research Hospital–Washington University Pediatric Cancer Genome Project, Targeting oxidative stress in embryonal rhabdomyosarcoma. Cancer Cell 24, 710–724 (2013). [PubMed: 24332040]
9. Shern JF, Chen L, Chmielecki J, Wei JS, Patidar R, Rosenberg M, Ambrogio L, Auclair D, Wang J, Song YK, Tolman C, Hurd L, Liao H, Zhang S, Bogen D, Brohl AS, Sindiri S, Catchpoole D, Badgett T, Getz G, Mora J, Anderson JR, Skapek SX, Barr FG, Meyerson M, Hawkins DS, Khan J, Comprehensive genomic analysis of rhabdomyosarcoma reveals a landscape of alterations affecting a common genetic axis in fusion-positive and fusion-negative tumors. Cancer Discov 4, 216–231 (2014). [PubMed: 24436047]

10. Chen L, Shern JF, Wei JS, Yohe ME, Song YK, Hurd L, Liao H, Catchpoole D, Skapek SX, Barr FG, Hawkins DS, Khan J, Clonality and evolutionary history of rhabdomyosarcoma. PLOS Genet 11, e1005075 (2015). [PubMed: 25768946]
11. Li Z, Zhang Y, Ramanujan K, Ma Y, Kirsch DG, Glass DJ, Oncogenic NRAS, required for pathogenesis of embryonic rhabdomyosarcoma, relies upon the HMGA2–IGF2BP2 pathway. Cancer Res 73, 3041–3050 (2013). [PubMed: 23536553]
12. Blum JM, Añó L, Li Z, Van Mater D, Bennett BD, Sachdeva M, Lagutina I, Zhang M, Mito JK, Dodd LG, Cardona DM, Dodd RD, Williams N, Ma Y, Lepper C, Linardic CM, Mukherjee S, Grosveld GC, Fan C-M, Kirsch DG, Distinct and overlapping sarcoma subtypes initiated from muscle stem and progenitor cells. Cell Rep 5, 933–940 (2013). [PubMed: 24239359]
13. Hettmer S, Liu J, Miller CM, Lindsay MC, Sparks CA, Guertin DA, Bronson RT, Langenau DM, Wagers AJ, Sarcomas induced in discrete subsets of prospectively isolated skeletal muscle cells. Proc. Natl. Acad. Sci. U.S.A 108, 20002–20007 (2011). [PubMed: 22135462]
14. Kirsch DG, Dinulescu DM, Miller JB, Grimm J, Santiago PM, Young NP, Nielsen GP, Quade BJ, Chaber CJ, Schultz CP, Takeuchi O, Bronson RT, Crowley D, Korsmeyer SJ, Yoon SS, Hornicek FJ, Weissleder R, Jacks T, A spatially and temporally restricted mouse model of soft tissue sarcoma. Nat. Med 13, 992–997 (2007). [PubMed: 17676052]
15. Langenau DM, Keefe MD, Storer NY, Guyon JR, Kutok JL, Le X, Goessling W, Neuberg DS, Kunkel LM, Zon LI, Effects of RAS on the genesis of embryonal rhabdomyosarcoma. Genes Dev 21,1382–1395 (2007). [PubMed: 17510286]
16. Le X, Pugach EK, Hettmer S, Storer NY, Liu J, Wills AA, DiBiase A, Chen EY, Ignatius MS, Poss KD, Wagers AJ, Langenau DM, Zon LI, A novel chemical screening strategy in zebrafish identifies common pathways in embryogenesis and rhabdomyosarcoma development. Development 140, 2354–2364 (2013). [PubMed: 23615277]
17. Linardic CM, Downie DL, Qualman S, Bentley RC, Counter CM, Genetic modeling of human rhabdomyosarcoma. Cancer Res 65, 4490–4495 (2005). [PubMed: 15930263]
18. McKinnon T, Venier R, Dickson BC, Kabaroff L, Alkema M, Chen L, Shern JF, Yohe ME, Khan J, Gladdy RA, Kras activation in p53-deficient myoblasts results in high-grade sarcoma formation with impaired myogenic differentiation. Oncotarget 6, 14220–14232 (2015). [PubMed: 25992772]
19. Tsumura H, Yoshida T, Saito H, Imanaka-Yoshida K, Suzuki N, Cooperation of oncogenic K-ras and p53 deficiency in pleomorphic rhabdomyosarcoma development in adult mice. Oncogene 25, 7673–7679 (2006). [PubMed: 16785989]
20. Chen EY, DeRan MT, Ignatius MS, Grandinetti KB, Clagg R, McCarthy KM, Lobbardi RM, Brockmann J, Keller C, Wu X, Langenau DM, Glycogen synthase kinase 3 inhibitors induce the canonical WNT/beta-catenin pathway to suppress growth and self-renewal in embryonal rhabdomyosarcoma. Proc. Natl. Acad. Sci. U.S A 111, 5349–5354 (2014). [PubMed: 24706870]
21. Wright CJ, McCormack PL, Trametinib: First global approval. Drugs 73, 1245–1254 (2013). [PubMed: 23846731]
22. DeChant AK, Dee K, Weyman CM, Raf-induced effects on the differentiation and apoptosis of skeletal myoblasts are determined by the level of Raf signaling: Abrogation of apoptosis by Raf is downstream of caspase 3 activation. Oncogene 21, 5268–5279 (2002). [PubMed: 12149648]
23. Dorman CM, Johnson SE, Activated Raf inhibits avian myogenesis through a MAPK-dependent mechanism. Oncogene 18, 5167–5176 (1999). [PubMed: 10498866]
24. Dorman CM, Johnson SE, Activated Raf inhibits myogenesis through a mechanism independent of activator protein 1-mediated myoblast transformation. J. Biol. Chem 275, 27481–27487 (2000). [PubMed: 10867013]
25. Johnson SE, Dorman CM, Bolanowski SA, Inhibition of myogenin expression by activated Raf is not responsible for the block to avian myogenesis. J. Biol. Chem 277, 28742–28748 (2002). [PubMed: 12042315]
26. Chen J, Wang Y, Hamed M, Lacroix N, Li Q, Molecular basis for the regulation of transcriptional coactivator p300 in myogenic differentiation. Sci. Rep 5, 13727 (2015). [PubMed: 26354606]
27. Jiang B-H, Zheng JZ, Vogt PK, An essential role of phosphatidylinositol 3-kinase in myogenic differentiation. Proc. Natl. Acad. Sci. U.SA 95, 14179–14183 (1998).

28. Yue F, Bi P, Wang C, Li J, Liu X, Kuang S, Conditional loss of Pten in myogenic progenitors leads to postnatal skeletal muscle hypertrophy but age-dependent exhaustion of satellite cells. Cell Rep 17, 2340–2353 (2016). [PubMed: 27880908]
29. Ramocki MB, White MA, Konieczny SF, Taparowsky EJ, A role for RalGDS and a novel Ras effector in the Ras-mediated inhibition of skeletal myogenesis. J. Biol. Chem 273, 17696–17701 (1998). [PubMed: 9651367]
30. Hinson AR, Jones R, Crose LE, Belyea BC, Barr FG, Linardic CM, Human rhabdomyosarcoma cell lines for rhabdomyosarcoma research: Utility and pitfalls. Front. Oncol 3, 183 (2013). [PubMed: 23882450]
31. Mathews Griner LA, Guha R, Shinn P, Young RM, Keller JM, Liu D, Goldlust IS, Yasgar A, McKnight C, Boxer MB, Duveau DY, Jiang J-K, Michael S, Mierzwa T, Huang W, Walsh MJ, Mott BT, Patel P, Leister W, Maloney DJ, Leclair CA, Rai G, Jadhav A, Peyser BD, Austin CP, Martin SE, Simeonov A, Ferrer M, Staudt LM, Thomas CJ, High-throughput combinatorial screening identifies drugs that cooperate with ibrutinib to kill activated B-cell-like diffuse large B-cell lymphoma cells. Proc. Natl. Acad. Sci. U.S.A 111, 2349–2354 (2014). [PubMed: 24469833]
32. Ciccarelli C, Marampon F, Scoglio A, Mauro A, Giacinti C, De Cesaris P, Zani BM, p21WAF1 expression induced by MEK/ERK pathway activation or inhibition correlates with growth arrest, myogenic differentiation and onco-phenotype reversal in rhabdomyosarcoma cells. Mol. Cancer 4, 41 (2005). [PubMed: 16351709]
33. Trapnell C, Cacchiarelli D, Grimsby J, Pokharel P, Li S, Morse M, Lennon NJ, Livak KJ, Mikkelsen TS, Rinn JL, The dynamics and regulators of cell fate decisions are revealed by pseudotemporal ordering of single cells. Nat. Biotechnol 32, 381–386 (2014). [PubMed: 24658644]
34. Sears RC, The life cycle of C-myc: From synthesis to degradation. Cell Cycle 3, 1133–1137 (2004). [PubMed: 15467447]
35. Tang Z, Dai S, He Y, Doty RA, Shultz LD, Sampson SB, Dai C, MEK guards proteome stability and inhibits tumor-suppressive amyloidogenesis via HSF1. Cell 160, 729–744 (2015). [PubMed: 25679764]
36. Chaikuad A, Tacconi EM, Zimmer J, Liang Y, Gray NS, Tarsounas M, Knapp S, A unique inhibitor binding site in ERK1/2 is associated with slow binding kinetics. Nat. Chem. Biol 10, 853–860 (2014). [PubMed: 25195011]
37. Göke J, Chan YS, Yan J, Vingron M, Ng HH, Genome-wide kinase-chromatin interactions reveal the regulatory network of ERK signaling in human embryonic stem cells. Mol. Cell50, 844–855 (2013). [PubMed: 23727019]
38. Tee W-W, Shen SS, Oksuz O, Narendra V, Reinberg D, Erk1/2 activity promotes chromatin features and RNAPII phosphorylation at developmental promoters in mouse ESCs. Cell 156, 678–690 (2014). [PubMed: 24529373]
39. McLean CY, Bristor D, Hiller M, Clarke SL, Schaar BT, Lowe CB, Wenger AM, Bejerano G, GREAT improves functional interpretation of cis-regulatory regions. Nat. Biotechnol 28, 495–501 (2010). [PubMed: 20436461]
40. Huang da W, Sherman BT, Lempicki RA, Systematic and integrative analysis of large gene lists using DAVID bioinformatics resources. Nat. Protoc 4, 44–57 (2009). [PubMed: 19131956]
41. Ciarapica R, Carcarino E, Adesso L, De Salvo M, Bracaglia G, Leoncini PP, Dall'agnese A, Verginelli F, Milano GM, Boldrini R, Inserra A, Stifani S, Screpanti I, Marquez VE, Valente S, Mai A, Puri PL, Locatelli F, Palacios D, Rota R, Pharmacological inhibition of EZH2 as a promising differentiation therapy in embryonal RMS. BMC Cancer 14, 139 (2014). [PubMed: 24575771]
42. Rahl PB, Lin CY, Seila AC, Flynn RA, McCuine S, Burge CB, Sharp PA, Young RA, c-Myc regulates transcriptional pause release. Cell 141, 432–445 (2010). [PubMed: 20434984]
43. Bentzinger CF, Wang YX, Rudnicki MA, Building muscle: Molecular regulation of myogenesis. Cold Spring Harb. Perspect. Biol 4, a008342 (2012). [PubMed: 22300977]
44. Lo TL, Fong CW, Yusoff P, McKie AB, Chua MS, Leung HY, Guy GR, Sprouty and cancer: The first terms report. Cancer Lett 242, 141–150 (2006). [PubMed: 16469433]

45. Kohsaka S, Shukla N, Ameur N, Ito T, Ng CK, Wang L, Lim D, Marchetti A, Viale A, Pirun M, Socci ND, Qin LX, Sciot R, Bridge J, Singer S, Meyers P, Wexler LH, Barr FG, Dogan S, Fletcher JA, Reis-Filho JS, Ladanyi M, A recurrent neomorphic mutation in MYOD1 defines a clinically aggressive subset of embryonal rhabdomyosarcoma associated with PI3K-AKT pathway mutations. Nat. Genet 46, 595–600 (2014). [PubMed: 24793135]
46. Miner JH, Wold BJ, c-myc Inhibition of MyoD and myogenin-initiated myogenic differentiation. Mol. Cell. Biol 11, 2842–2851 (1991). [PubMed: 1850105]
47. Ernst J, Kheradpour P, Mikkelsen TS, Shoresh N, Ward LD, Epstein CB, Zhang X, Wang L, Issner R, Coyne M, Ku M, Durham T, Kellis M, Bernstein BE, Mapping and analysis of chromatin state dynamics in nine human cell types. Nature 473, 43–49 (2011). [PubMed: 21441907]
48. Lin CY, Loven J, Rahl PB, Paranal RM, Burge CB, Bradner JE, Lee TI, Young RA, Transcriptional amplification in tumor cells with elevated c-Myc. Cell 151, 56–67 (2012). [PubMed: 23021215]
49. Cao Y, Yao Z, Sarkar D, Lawrence M, Sanchez GJ, Parker MH, MacQuarrie KL, Davison J, Morgan MT, Ruzzo WL, Gentleman RC, Tapscott SJ, Genome-wide MyoD binding in skeletal muscle cells: A potential for broad cellular reprogramming. Dev. Cell 18, 662–674 (2010). [PubMed: 20412780]
50. MacQuarrie KL, Yao Z, Fong AP, Diede SJ, Rudzinski ER, Hawkins DS, Tapscott SJ, Comparison of genome-wide binding of MyoD in normal human myogenic cells and rhabdomyosarcomas identifies regional and local suppression of promyogenic transcription factors. Mol. Cell. Biol 33, 773–784 (2013). [PubMed: 23230269]
51. Gryder BE, Yohe ME, Chou H-C, Zhang X, Marques J, Wachtel M, Schaefer B, Sen N, Song Y, Gualtieri A, Pomella S, Rota R, Cleveland A, Wen X, Sindiri S, Wei JS, Barr FG, Das S, Andresson T, Guha R, Lal-Nag M, Ferrer M, Shern JF, Zhao K, Thomas CJ, Khan J, PAX3-FOXO1 establishes myogenic super enhancers and confers BET bromodomain vulnerability. CancerDiscov 7, 884–899 (2017).
52. Chapuy B, McKeown MR, Lin CY, Monti S, Roemer MG, Qi J, Rahl PB, Sun HH, Yeda KT, Doench JG, Reichert E, Kung AL, Rodig SJ, Young RA, Shipp MA, Bradner JE, Discovery and characterization of super-enhancer-associated dependencies in diffuse large B cell lymphoma. Cancer Cell 24, 777–790 (2013). [PubMed: 24332044]
53. Lin CY, Erkek S, Tong Y, Yin L, Federation AJ, Zapatka M, Haldipur P, Kawauchi D, Risch T, Warnatz H-J, Worst BC, Ju B, Orr BA, Zeid R, Polaski DR, Segura-Wang M, Waszak SM, Jones DT, Kool M, Hovestadt V, Buchhalter I, Sieber L, Johann P, Chavez L, Gröschel S, Ryzhova M, Korshunov A, Chen W, Chizhikov VV, Millen KJ, Amstislavskiy V, Lehrach H, Yaspo M-L, Eils R, Lichter P, Korbel JO, Pfister SM, Bradner JE, Northcott PA, Active medulloblastoma enhancers reveal subgroup-specific cellular origins. Nature 530, 57–62 (2016). [PubMed: 26814967]
54. Pratilas CA, Taylor BS, Ye Q, Viale A, Sander C, Solit DB, Rosen N, ^{V600E}BRAF is associated with disabled feedback inhibition of RAF-MEK signaling and elevated transcriptional output of the pathway. Proc. Natl. Acad. Sci. U.S.A 106, 4519–4524 (2009). [PubMed: 19251651]
55. ENCODE Project Consortium, An integrated encyclopedia of DNA elements in the human genome. Nature 489, 57–74 (2012). [PubMed: 22955616]
56. Svalina MN, Keller C, YAPping about differentiation therapy in muscle cancer. Cancer Cell 26, 154–155 (2014). [PubMed: 25117705]
57. Renshaw J, Taylor KR, Bishop R, Valenti M, De Haven Brandon A, Gowan S, Eccles SA, Ruddle RR, Johnson LD, Raynaud FI, Selfe JL, Thway K, Pietsch T, Pearson AD, Shipley J, Dual blockade of the PI3K/AKT/mTOR (AZD8055) and RAS/MEK/ERK (AZD6244) pathways synergistically inhibits rhabdomyosarcoma cell growth in vitro and in vivo. Clin. Cancer Res 19, 5940–5951 (2013). [PubMed: 23918606]
58. Ebi H, Corcoran RB, Singh A, Chen Z, Song Y, Lifshits E, Ryan DP, Meyerhardt JA, Benes C, Settleman J, Wong K-K, Cantley LC, Engelman JA, Receptor tyrosine kinases exert dominant control over PI3K signaling in human KRAS mutant colorectal cancers. J. Clin. Invest 121,4311–4321 (2011). [PubMed: 21985784]
59. Flanigan SA, Pitts TM, Newton TP, Kulikowski GN, Tan AC, McManus MC, Spreafico A, Kachaeva MI, Selby HM, Tentler JJ, Eckhardt SG, Leong S, Overcoming IGF1R/IR resistance through inhibition of MEK signaling in colorectal cancer models. Clin. Cancer Res 19, 6219–6229 (2013). [PubMed: 24045180]

60. Molina-Arcas M, Hancock DC, Sheridan C, Kumar MS, Downward J, Coordinate direct input of both KRAS and IGF1 receptor to activation of PI3 kinase in KRAS-mutant lung cancer. Cancer Discov 3, 548–563 (2013). [PubMed: 23454899]
61. Weisberg E, Nonami A, Chen Z, Nelson E, Chen Y, Liu F, Cho H, Zhang J, Sattler M, Mitsiades C, Wong KK, Liu Q, Gray NS, Griffin JD, Upregulation of IGF1R by mutant RAS in leukemia and potentiation of RAS signaling inhibitors by small-molecule inhibition of IGF1R. Clin. Cancer Res 20, 5483–5495 (2014). [PubMed: 25186968]
62. Dry JR, Pavey S, Pratilas CA, Harbron C, Runswick S, Hodgson D, Chresta C, McCormack R, Byrne N, Cockerill M, Graham A, Beran G, Cassidy A, Haggerty C, Brown H, Ellison G, Dering J, Taylor BS, Stark M, Bonazzi V, Ravishankar S, Packer L, Xing F, Solit DB, Finn RS, Rosen N, Hayward NK, French T, Smith PD, Transcriptional pathway signatures predict MEK addiction and response to selumetinib (AZD6244). Cancer Res 70, 2264–2273 (2010). [PubMed: 20215513]
63. Nabet B, Broin PÓ, Reyes JM, Shieh K, Lin CY, Will CM, Popovic R, Ezponda T, Bradner JE, Golden AA, Licht JD, Deregulation of the Ras-Erk signaling axis modulates the enhancer landscape. Cell Rep 12, 1300–1313 (2015). [PubMed: 26279576]
64. Hnisz D, Schuijers J, Lin CY, Weintraub AS, Abraham BJ, Lee TI, Bradner JE, Young RA, Convergence of developmental and oncogenic signaling pathways at transcriptional super-enhancers. Mol. Cell 58, 362–370 (2015). [PubMed: 25801169]
65. Bennett AM, Tonks NK, Regulation of distinct stages of skeletal muscle differentiation by mitogen-activated protein kinases. Science 278, 1288–1291 (1997). [PubMed: 9360925]
66. Winter B, Arnold HH, Activated raf kinase inhibits muscle cell differentiation through a MEF2-dependent mechanism. J. Cell Sci 113 (Pt 23), 4211–4220 (2000). [PubMed: 11069766]
67. Perry RL, Parker MH, Rudnicki MA, Activated MEK1 binds the nuclear MyoD transcriptional complex to repress transactivation. Mol. Cell 8, 291–301 (2001). [PubMed: 11545732]
68. Michailovici I, Harrington HA, Azogui HH, Yahalom-Ronen Y, Plotnikov A, Ching S, Stumpf MP, Klein OD, Seger R, Tzahor E, Nuclear to cytoplasmic shuttling of ERK promotes differentiation of muscle stem/progenitor cells. Development 141,2611–2620 (2014). [PubMed: 24924195]
69. Li J, Johnson SE, ERK2 is required for efficient terminal differentiation of skeletal myoblasts. Biochem. Biophys. Res. Commun 345, 1425–1433 (2006). [PubMed: 16729973]
70. Seaberg B, Henslee G, Wang S, Paez-Colasante X, Landreth GE, Rimer M, Muscle-derived extracellular signal-regulated kinases 1 and 2 are required for the maintenance of adult myofibers and their neuromuscular junctions. Mol. Cell. Biol 35, 1238–1253 (2015). [PubMed: 25605336]
71. Marampon F, Bossi G, Ciccarelli C, Di Rocco A, Sacchi A, Pestell RG, Zani BM, MEK/ERK inhibitor U0126 affects in vitro and in vivo growth of embryonal rhabdomyosarcoma. Mol. Cancer Ther 8, 543–551 (2009). [PubMed: 19258428]
72. Marampon F, Ciccarelli C, Zani BM, Down-regulation of c-Myc following MEK/ERK inhibition halts the expression of malignant phenotype in rhabdomyosarcoma and in non muscle-derived human tumors. Mol. Cancer 5, 31 (2006). [PubMed: 16899113]
73. Schaaf G, Hamdi M, Zwijnenburg D, Lakeman A, Geerts D, Versteeg R, Kool M, Silencing of SPRY1 triggers complete regression of rhabdomyosarcoma tumors carrying a mutated RAS gene. Cancer Res 70, 762–771 (2010). [PubMed: 20068162]
74. Teicher BA, Polley E, Kunkel M, Evans D, Silvers T, Delosh R, Laudeman J, Ogle C, Reinhart R, Selby M, Connelly J, Harris E, Monks A, Morris J, Sarcoma cell line screen of oncology drugs and investigational agents identifies patterns associated with gene and microRNA expression. Mol. Cancer Ther 14, 2452–2462 (2015). [PubMed: 26351324]
75. Xu J, Haigis KM, Firestone AJ, McNerney ME, Li Q, Davis E, Chen S-C, Nakitandwe J, Downing J, Jacks T, Le Beau MM, Shannon K, Dominant role of oncogene dosage and absence of tumor suppressor activity in Nras-driven hematopoietic transformation. Cancer Discov 3, 993–1001 (2013). [PubMed: 23733505]
76. Ceribelli M, Kelly PN, Shaffer AL, Wright GW, Xiao W, Yang Y, Mathews Griner LA, Guha R, Shinn P, Keller JM, Liu D, Patel PR, Ferrer M, Joshi S, Nerle S, Sandy P, Normant E, Thomas CJ, Staudt LM, Blockade of oncogenic IκB kinase activity in diffuse large B-cell lymphoma by bromodomain and extraterminal domain protein inhibitors. Proc. Natl. Acad. Sci. U.S.A 111, 11365–11370 (2014). [PubMed: 25049379]

77. Young A, Lou D, McCormick F, Oncogenic and wild-type Ras play divergent roles in the regulation of mitogen-activated protein kinase signaling. Cancer Discov 3, 112–123 (2013). [PubMed: 23103856]

78. Gilmartin AG, Bleam MR, Groy A, Moss KG, Minthorn EA, Kulkarni SG, Rominger CM, Erskine S, Fisher KE, Yang J, Zappacosta F, Annan R, Sutton D, Laquerre SG, GSK1120212 (JTP-74057) is an inhibitor of MEK activity and activation with favorable pharmacokinetic properties for sustained in vivo pathway inhibition. Cancer Res 17, 989–1000 (2011).

79. Hou X, Huang F, Macedo LF, Harrington SC, Reeves KA, Greer A, Finckenstein FG, Brodie A, Gottardis MM, Carboni JM, Haluska P, Dual IGF-1R/InsR inhibitor BMS-754807 synergizes with hormonal agents in treatment of estrogen-dependent breast cancer. Cancer Res 71, 7597–7607 (2011). [PubMed: 22042792]

80. Khanna C, Prehn J, Yeung C, Caylor J, Tsokos M, Helman L, An orthotopic model of murine osteosarcoma with clonally related variants differing in pulmonary metastatic potential. Clin. Exp. Metastasis 18, 261–271 (2000). [PubMed: 11315100]

81. Zhang Y, Liu T, Meyer CA, Eeckhoute J, Johnson DS, Bernstein BE, Nusbaum C, Myers RM, Brown M, Li W, Liu XS, Model-based analysis of ChIP-Seq (MACS). Genome Biol 9, R137 (2008). [PubMed: 18798982]

82. Heinz S, Benner C, Spann N, Bertolino E, Lin YC, Laslo P, Cheng JX, Murre C, Singh H, Glass CK, Simple combinations of lineage-determining transcription factors prime cis-regulatory elements required for macrophage and B cell identities. Mol. Cell 38, 576–589 (2010). [PubMed: 20513432]

83. Ernst J, Kellis M, ChromHMM: Automating chromatin-state discovery and characterization. Nat. Methods 9, 215–216 (2012). [PubMed: 22373907]

84. Whyte WA, Orlando DA, Hnisz D, Abraham BJ, Lin CY, Kagey MH, Rahl PB, Lee TI, Young RA, Master transcription factors and mediator establish super-enhancers at key cell identity genes. Cell 153, 307–319 (2013). [PubMed: 23582322]

85. Quinlan AR, Hall IM, BEDTools: A flexible suite of utilities for comparing genomic features. Bioinformatics 26, 841–842 (2010). [PubMed: 20110278]

86. Shen L, Shao N, Liu X, Nestler E, ngs.plot: Quick mining and visualization of next-generation sequencing data by integrating genomic databases. BMC Genomics 15, 284 (2014). [PubMed: 24735413]

87. Orlando DA, Chen MW, Brown VE, Solanki S, Choi YJ, Olson ER, Fritz CC, Bradner JE, Guenther MG, Quantitative ChIP-seq normalization reveals global modulation of the epigenome. Cell Rep 9, 1163–1170 (2014). [PubMed: 25437568]

88. Chang W, Brohl A, Patidar R, Sindiri S, Shern JF, Wei JS, Song YK, Yohe ME, Gryder BE, Zhang S, Calzone KA, Shivaprasad N, Wen X, Badgett T, Miettinen M, Hartman KR, League-Pascual JC, Trahair T, Widemann BC, Merchant MS, Kaplan RN, Lin JC, Khan J, Multi-dimensional ClinOmics for precision therapy of children and adolescent young adults with relapsed and refractory cancer: A report from the Center for Cancer Research. Clin. Cancer Res (2016).

89. Jin W, Tang Q, Wan M, Cui K, Zhang Y, Ren G, Ni B, Sklar J, Przytycka TM, Childs R, Levens D, Zhao K, Genome-wide detection of DNase I hypersensitive sites in single cells and FFPE tissue samples. Nature 528, 142–146 (2015). [PubMed: 26605532]

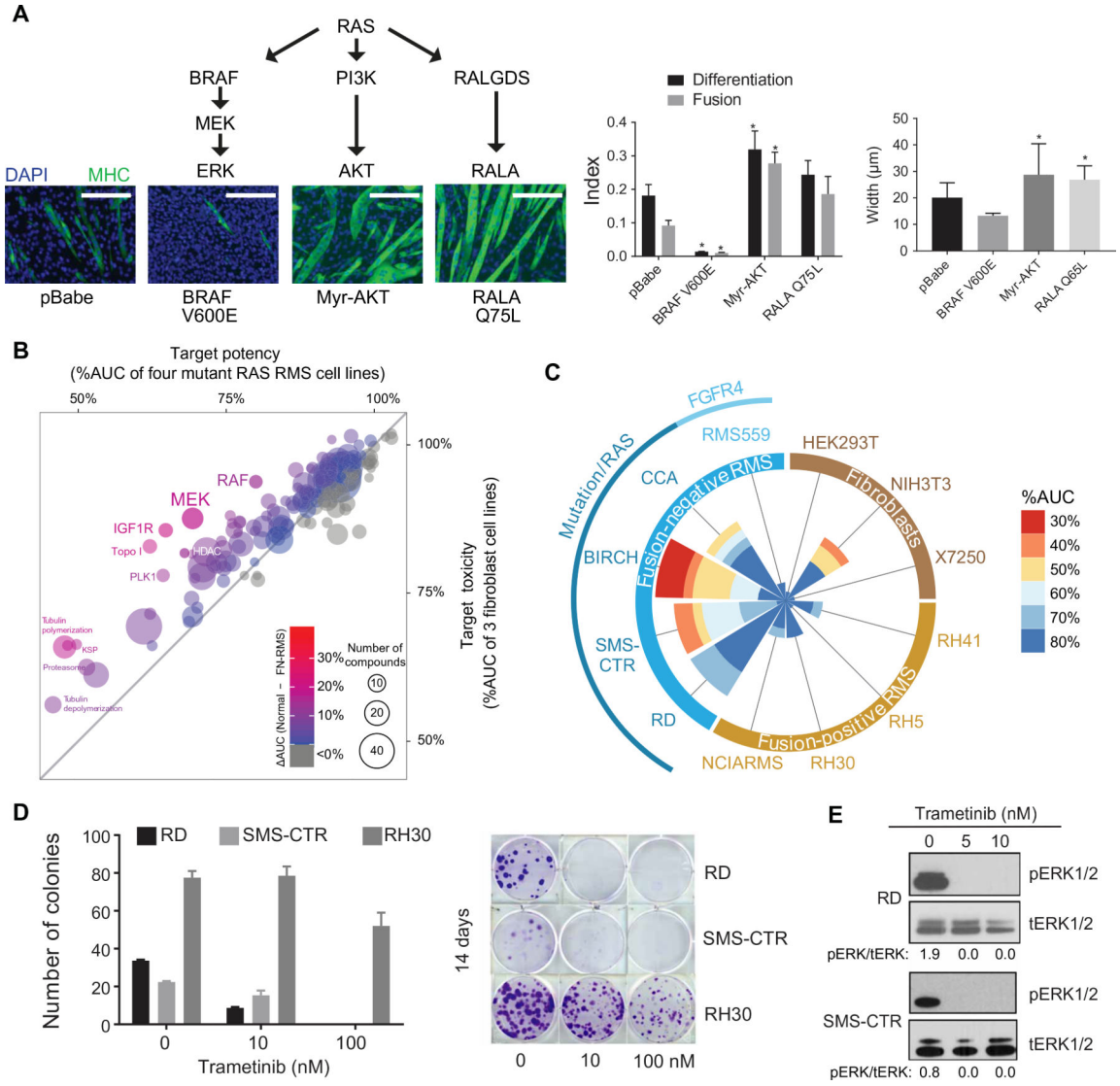

Fig. 1. MEK inhibitors potently and selectively decrease cell viability in FN-RMS.

(**A**) Expression of BRAF V600E—but not the empty vector control (pBABE), Myr-AKT, or RALA Q75L—inhibits differentiation of C2C12 myoblasts serum-starved for 5 days as determined by immunofluorescence for myosin heavy chain (MHC). Scale bars, 200 μm. Quantification of differentiation index, fusion index, and myocyte width is shown at right. Data are means ± SD for 3 representative fields (indices) or 10 representative myocytes (myocyte width). **P* < 0.05. (**B**) A bubble plot comparing the potency of the classes of compounds found in the MIPE-v4 screen in FN-RMS cell lines with potency in normal cell lines. Each bubble represents a class of drugs; the size of the bubble is proportional to the number of drugs in that class; and the color of the bubble corresponds to the potency of that class. Potency is represented as %AUC. HDAC, histone deacetylase; PLK1, Polo-like kinase; KSP, kinesin-like spindle protein. (**C**) A wind-rose plot shows that MEK inhibitors are potent and selective for FN-RMS, as compared to fusion-positive RMS (FP-RMS) and normal cell lines. Each cell line investigated corresponds to a spoke of the plot. The size of the wedge along each cell line spoke is proportional to the number of drugs in the class

displaying potency of 80% AUC or less. The wedges are colored on the basis of the %AUC of the drugs from red (30%) to blue (80%). FGFR4, fibroblast growth factor receptor 4; HEK293T, human embryonic kidney–293T cells. (**D**) Quantification (left) and representative images (right) of 14-day clonogenic assays for RD, SMS-CTR, and RH30 in the presence of trametinib. Data are means ± SD for three replicates. (**E**) Six hours of trametinib treatment decreases ERK phosphorylation in RD (top) and SMS-CTR (bottom) as determined by immunoblot. pERK, phosphorylated ERK; tERK, total ERK.

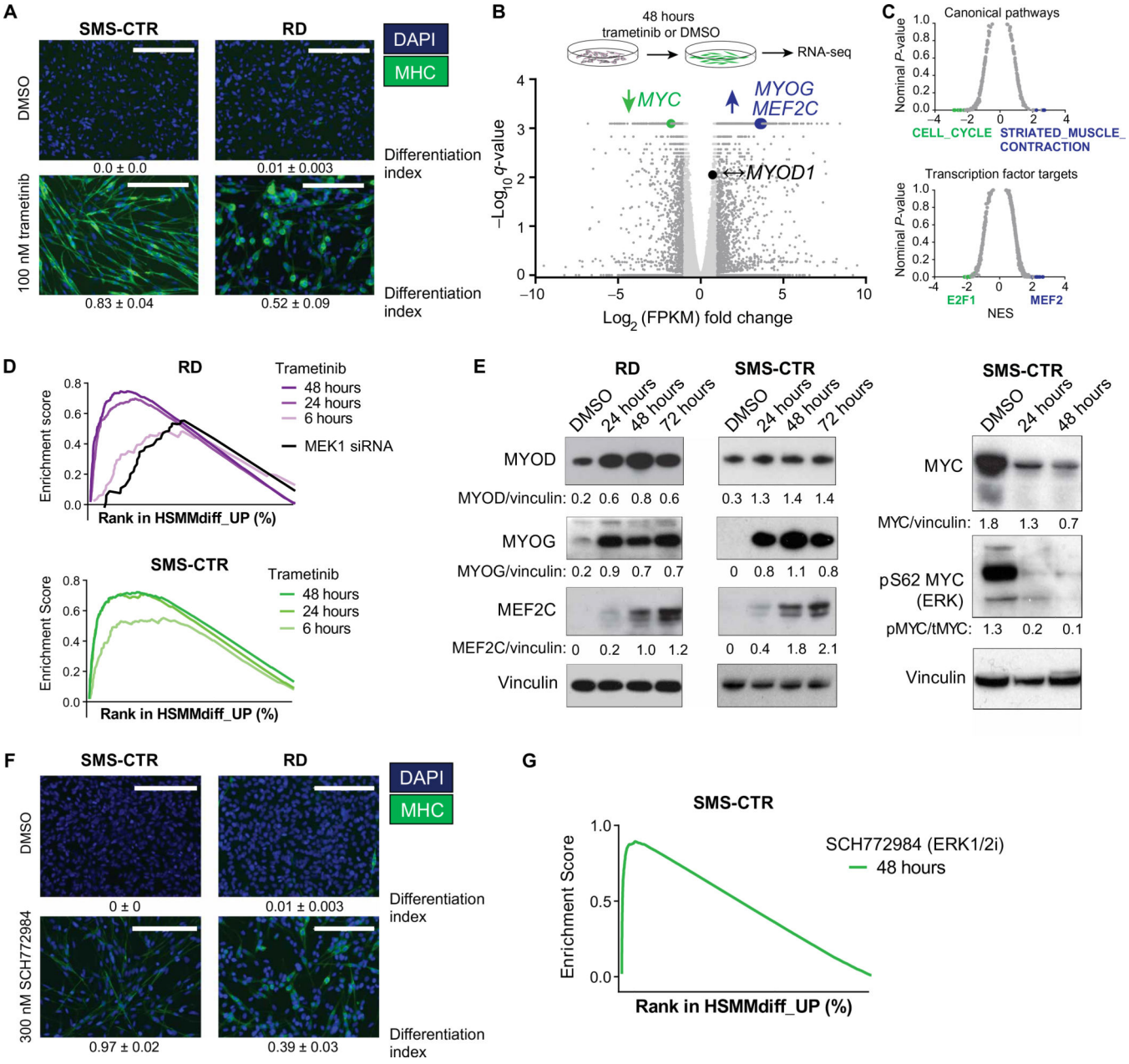

Fig. 2. MEK/ERK inhibition induces myogenic differentiation in FN-RMS.

(**A**) Treatment with 100 nM trametinib for 72 hours induces differentiation in SMS-CTR (left) and RD (right) cells grown in complete medium as determined by immunofluorescence for MHC. Scale bars, 200 μm. (**B**) Volcano plot comparing gene expression in SMS-CTR treated with 100 nM trametinib or vehicle for 48 hours. Statistically significant differentially expressed genes (at least twofold change with $P < 0.05$) are represented by dark gray dots; genes that are not differentially expressed are represented by light gray dots. Differential expression of *MYC* (green, decreased expression in trametinib-treated cells), *MYOG* and *MEF2C* (blue, increased expression in trametinib-treated cells), and *MYOD* (black, unchanged expression) is highlighted. (**C**) Significance (nominal *P* value) versus normalized

enrichment score (NES) plot for gene sets in the C2: canonical pathways molecular signatures database (top) and C3: transcription factor motif molecular signatures database (bottom). (**D**) Gene set enrichment analysis (GSEA) enrichment plot showing positive enrichment for a set of genes up-regulated during differentiation of human skeletal muscle myoblasts into myotubes in both RD (top) and SMS-CTR (bottom) treated with trametinib or transfected with MEK1 small interfering RNA (siRNA; RD only). For each of the enrichment plots shown here, the false discovery rate (FDR) q value and the nominal P value is < 0.05. (**E**) Expression of *MYOG* and *MEF2C* but not of *MYOD* is induced by trametinib treatment in RD (left) and SMS-CTR (right) as determined by immunoblot. Expression and phosphorylation of *MYC* are decreased by trametinib treatment in SMS-CTR as determined by immunoblot (far right). (**F**) ERK inhibition with 100 nM SCH772894 for 72 hours induces differentiation in SMS-CTR (left) and RD (right) cells grown in complete medium as determined by immunofluorescence for MHC. Scale bars, 200 μm. (**G**) GSEA enrichment plot showing positive enrichment for a set of genes up-regulated during differentiation of human skeletal muscle myoblasts into myotubes in SMS-CTR treated with the ERK inhibitor, SCH77894 (FDR and nominal $P < 0.05$).

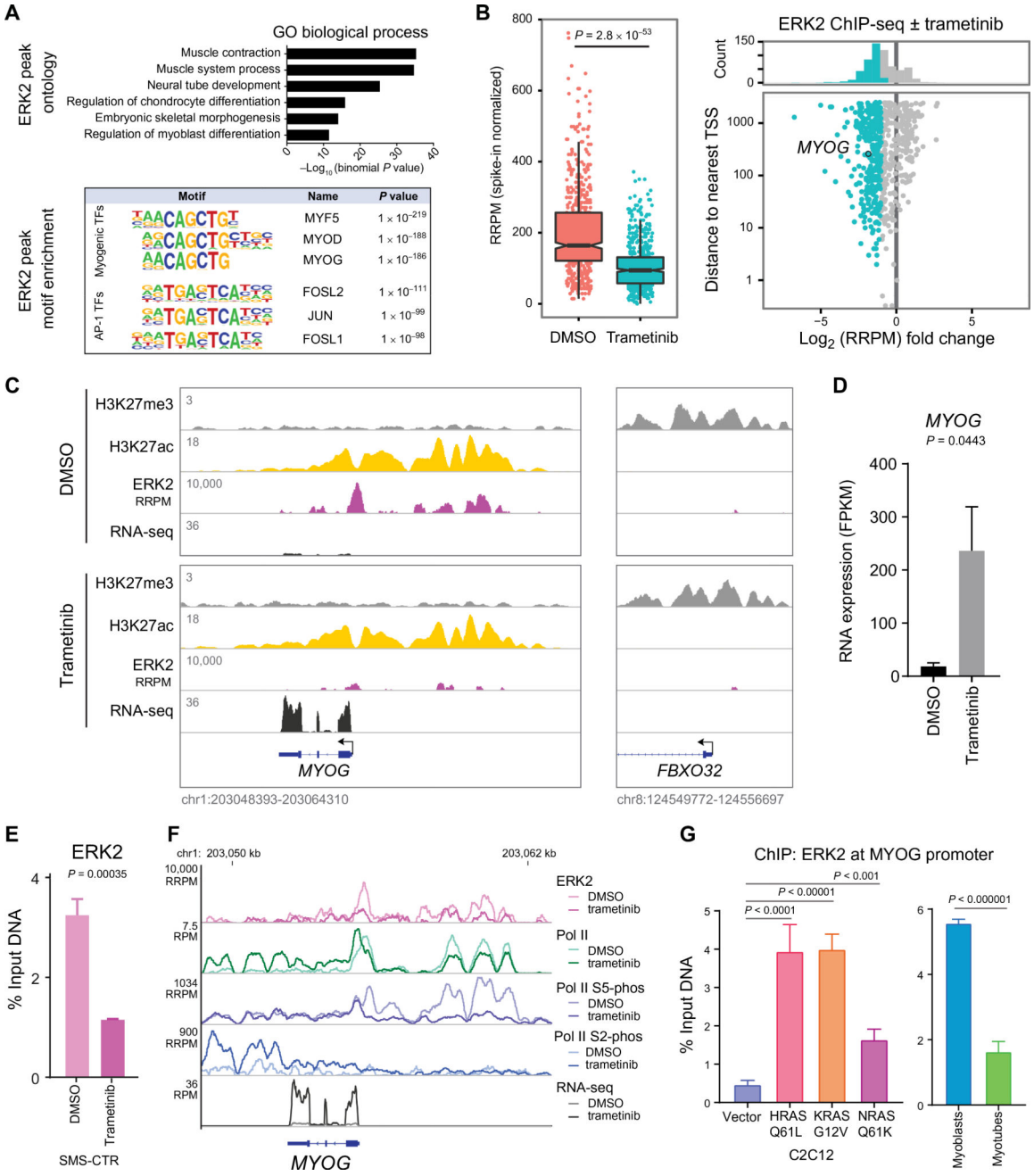

Fig. 3. ERK2 inhibits RMS differentiation by stalling transcription of *MYOG*.

(**A**) ERK2 peaks in SMS-CTR are enriched for pathways important for muscle contraction and development (top), and these peaks are enriched with binding motifs for myogenic and AP-1 transcription factors (bottom). GO, gene ontology. (**B**) Promoter-proximal ERK2 ChIP-seq peaks that decrease in signal intensity [reported as reference-adjusted reads per million mapped reads (RRPM)] with trametinib treatment, visualized as a box plot (left). The difference in ERK2 signal intensity with trametinib treatment is statistically significant (paired *t* test). The promoters for which there was a decrease greater than twofold in ERK2 signal intensity are colored teal in the scatter plot at right. The promoters of myogenic

transcription factors *MYOG* and *MEF2A* are highlighted. (**C**) Representative ChIP-seq tracks for H3K27me3 (gray), H3K27ac (yellow), and ERK2 (pink), as well as RNA-seq tracks at the *MYOG* locus (left) and the FBXO32 locus (right) in dimethlysulfoxide (DMSO; top) and trametinib-treated (bottom) SMS-CTR cells. (**D**) Expression of *MYOG* as determined by RNA-seq in SMS-CTR in the presence and absence of trametinib. Data are means ± SD for three replicates; *P* value generated from unpaired *t* test with Welch's correction. (**E**) ChIP–quantitative polymerase chain reaction (qPCR) for ERK2 at the *MYOG* promoter in SMS-CTR in the presence and absence of trametinib. Results are presented as percentage of input material. Data are means ± SD of three replicates; *P* value generated from unpaired *t* test. (**F**) Representative ChIP-seq tracks for ERK2 (pink), total RNA Pol II (green), S5-phosphorylated Pol II (purple), and S2-phosphorylated Pol II (blue), as well as RNA-seq (gray) tracks at the *MYOG* locus in the presence and absence of trametinib. (**G**) ChIP-qPCR for ERK2 at the *MYOG* promoter in C2C12 expressing mutant RAS isoforms (left) or during normal differentiation (right). Results are presented as percentage of input material. Data are means ± SD of three replicates; *P* values generated from unpaired *t* test.

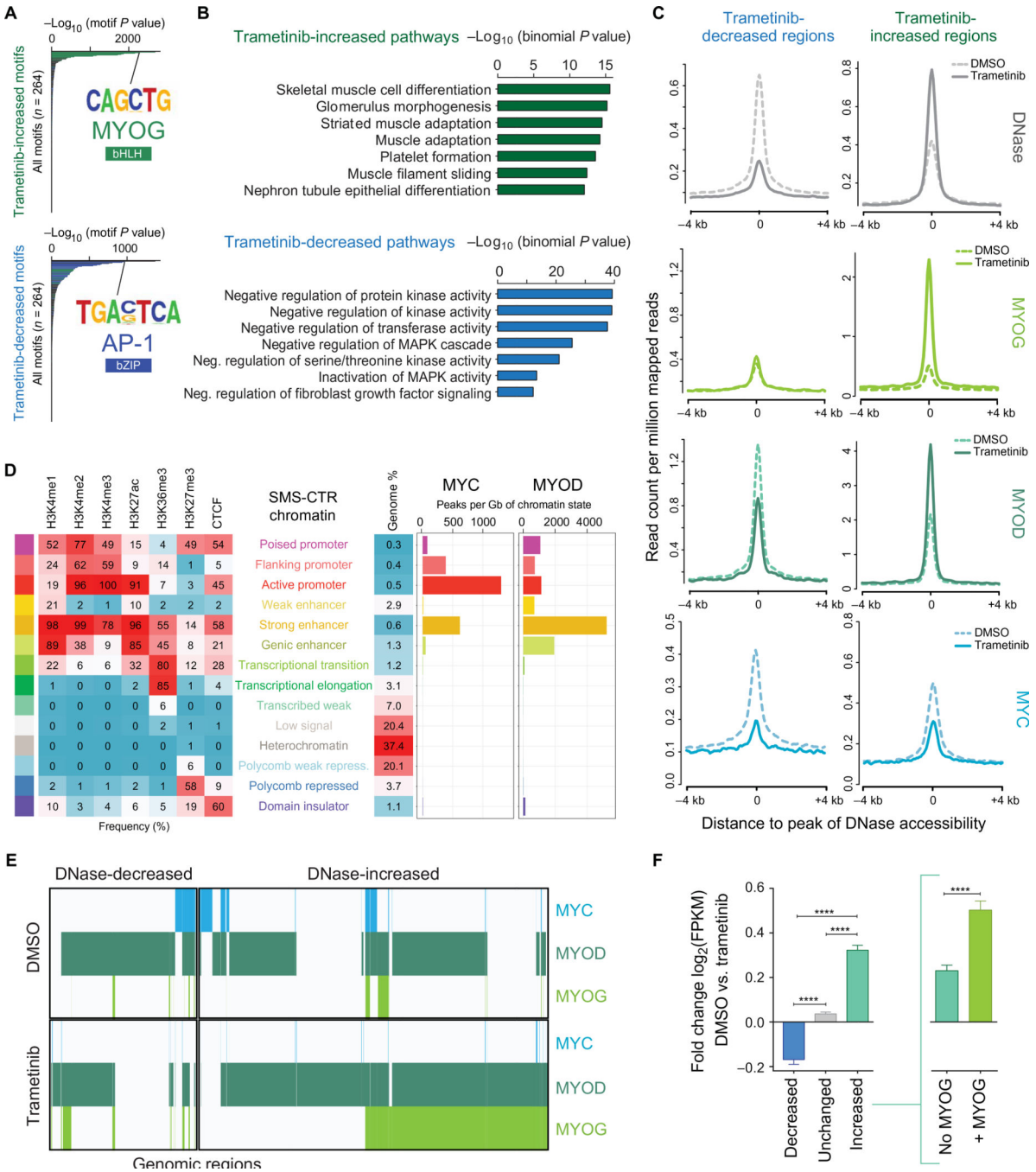

Fig. 4. Trametinib treatment induces chromatin reorganization in SMS-CTR.

(**A**) Hypergeometric Optimization of Motif Enrichment analysis reveals that regions with increased chromatin accessibility as a function of trametinib treatment are enriched with binding motifs for bHLH transcription factors (green) such as *MYOG,* among others (top), whereas trametinib-decreased regions are enriched with binding motifs for bZIP transcription factors (blue) such as AP-1, among others (bottom). (**B**) GREAT analysis shows that increased accessibility regions are enriched for pathways important for skeletal muscle development (green), among others (top), whereas decreased accessibility regions

are enriched for pathways important for the negative regulation of MAPK activity (blue), among others (bottom). (**C**) Composite plots showing DNase hypersensitivity (silver), *MYOG* (light green), *MYOD* (dark green), and *MYC* (blue) signal intensities (RPM) genome-wide in the presence and absence of trametinib treatment in SMS-CTR. (**D**) *MYC* and *MYOD* binding sites overlap enrichments of 12 chromatin states in SMS-CTR, defined by six histone modification marks and CTCF (CCCTC-binding factor). (**E**) Collaborative co-occupancy of *MYC* (blue), *MYOD* (dark green), and MYOG (light green) in the decreased and increased accessibility regions. The presence of each transcription factor at a given region is indicated by a colored line. (**F**) Bar charts representing the trametinib-induced fold change [log2(FPKM)] of the expression of genes nearest decreased (blue), unchanged (gray), and increased (aqua) accessibility regions. Increased accessibility regions are further subdivided into regions lacking *MYOG* deposition (aqua, inset at right) and regions with at least one overlapping *MYOG* peak (green). Error bars represent the 95% confidence interval. ****$P < 0.0001$, evaluated by Welch's *t* test.

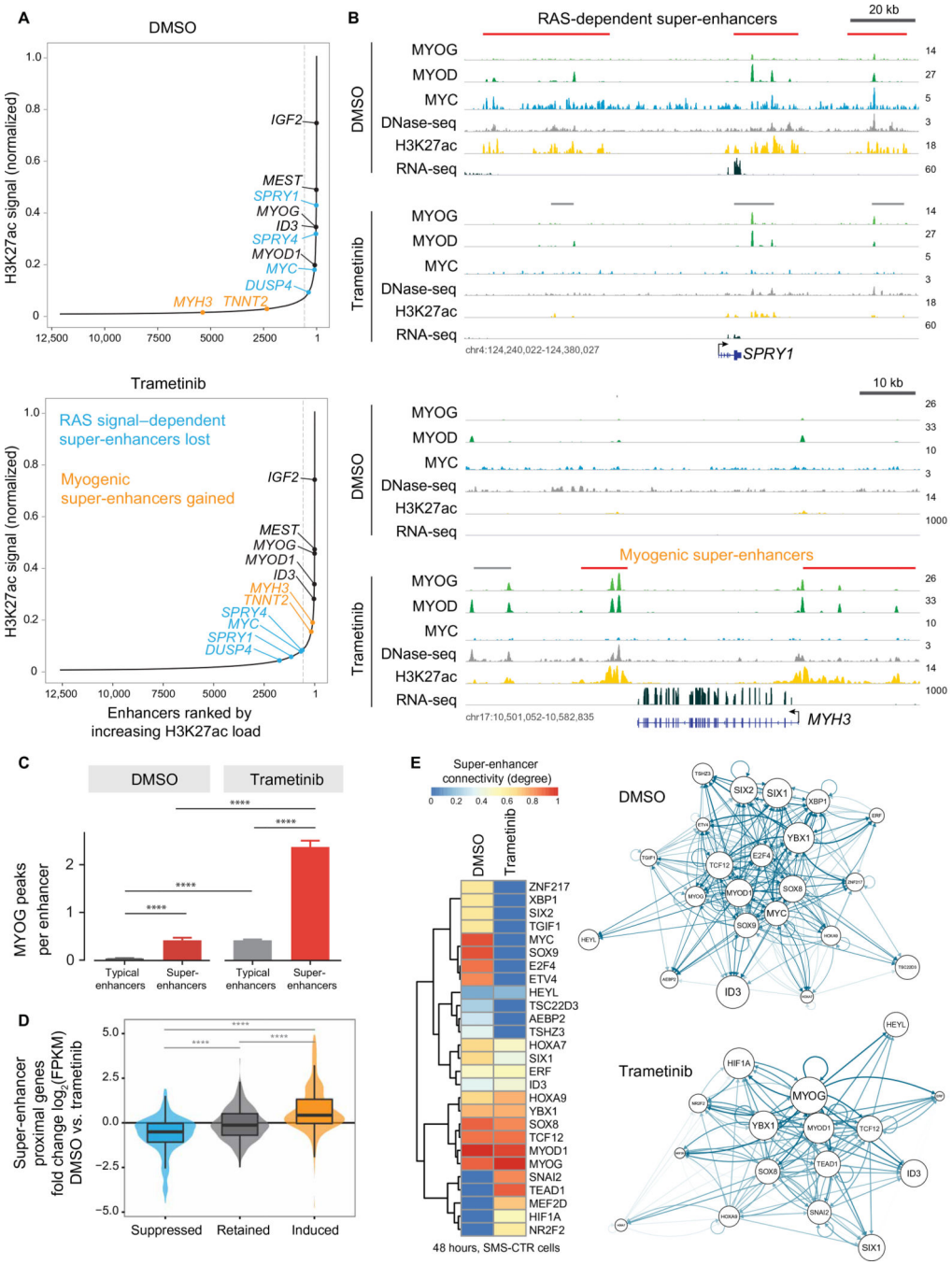

Fig. 5. Trametinib treatment remodels the super-enhancer landscape in SMS-CTR.

(**A**) Ranked order of H3K27ac-loaded enhancers in SMS-CTR treated with DMSO (top) or trametinib (bottom) reveals super-enhancers that are lost (blue), gained (gold), or unchanged (black) because of trametinib treatment. In these figures, the gray dashed line separates super-enchancers (right) from typical enhancers (left). A total of 571 super-enhancers were identified in DMSO-treated cells, and 577 were identified in cells treated with trametinib. (**B**) Signal tracks for *MYOG* (light green), *MYOD* (aqua), *MYC* (blue), and H3K27ac (yellow) ChIP-seq, DNAse sequencing (DNase-seq) (gray), and RNA-seq (dark green)

experiments performed on SMS-CTR treated with DMSO or trametinib for 48 hours at the *SPRY1* (Sprouty1; top) and *MYH3* (embryonic MHC 3; bottom) loci. Predicted typical enhancers are shown above the signal tracks for each condition in gray; super-enhancers are red. (**C**) Bar charts representing the number of MYOG peaks per enhancer in the absence and presence of trametinib. **** $P < 0.0001$, unpaired *t* test with Fisher's correction. (**D**) Violin plots depicting the trametinib-induced fold change [$\log_2$(FPKM)] of the expression of genes nearest the RAS-dependent, trametinib-decreased super-enhancers (blue), super-enhancers present in the absence and presence of trametinib (gray), and the myogenic, trametinib-induced super-enhancers (yel low). **** $P < 0.0001$, unpaired *t* test with Fisher's correction. (**E**) Heat map of super-enhancer-associated transcription factors in SMS-CTR in the absence (DMSO) and presence of trametinib, sorted by the change in total regulatory degree induced by trametinib treatment (left). The regulatory networks, as determined by COLTRON, are shown for DMSO-(right, top) and trametinib-treated (right, bottom) cells, highlighting the centrality of MYOG under the trametinib-treated condition.

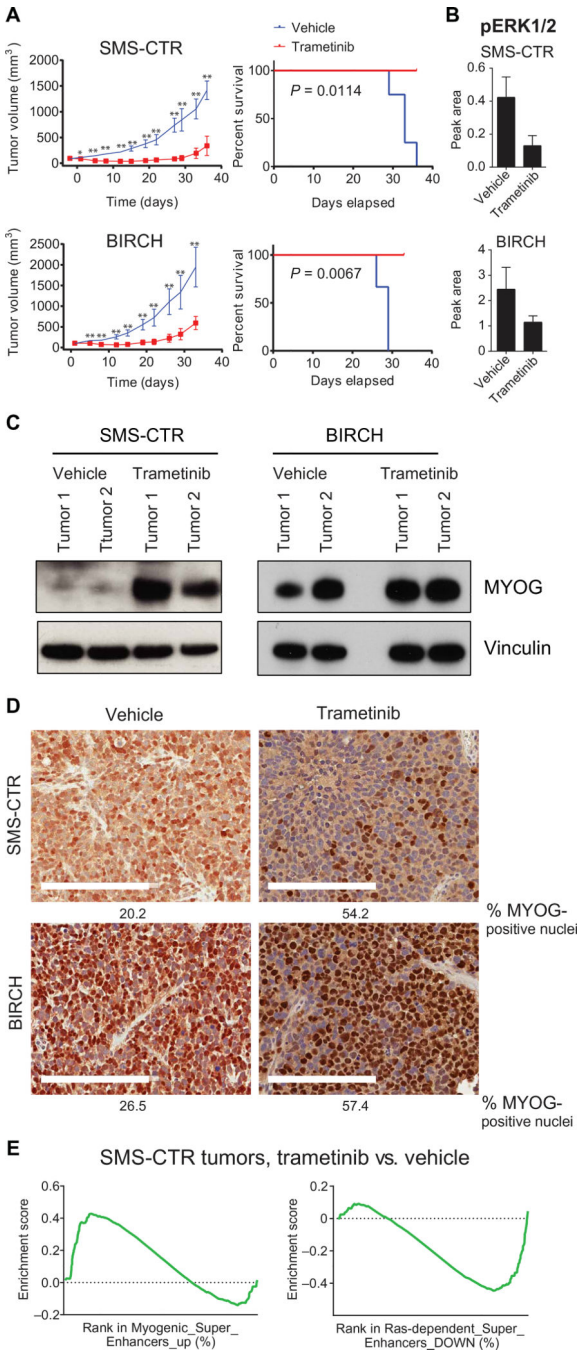

Fig. 6. Trametinib inhibits tumor growth and induces differentiation in xenograft models of FN-RMS.

(**A**) Daily trametinib inhibits tumor growth (left) and prolongs overall survival (right) in severe combined immunodeficient (SCID) Beige mice injected orthotopically with either SMS-CTR (top) or BIRCH (bottom) cell lines. $*P < 0.05$ and $**P < 0.01$, unpaired t test. (**B**) Trametinib decreases ERK phosphorylation in SMS-CTR and BIRCH xenografts as determined by capillary immunoassay. (**C**) Trametinib treatment increases *MYOG* expression in RD and SMS-CTR xenografts as determined by immunoblot and immunohistochemistry (**D**). Scale bars, 200 μm. (**E**) GSEA comparing gene expression of

SMS-CTR xenografts treated with either vehicle or trametinib shows positive enrichment of genes associated with MYOG-induced super-enhancers and negative enrichment of genes associated with RAS-dependent super-enhancers. FDR $q < 0.05$ and nominal $P < 0.01$.

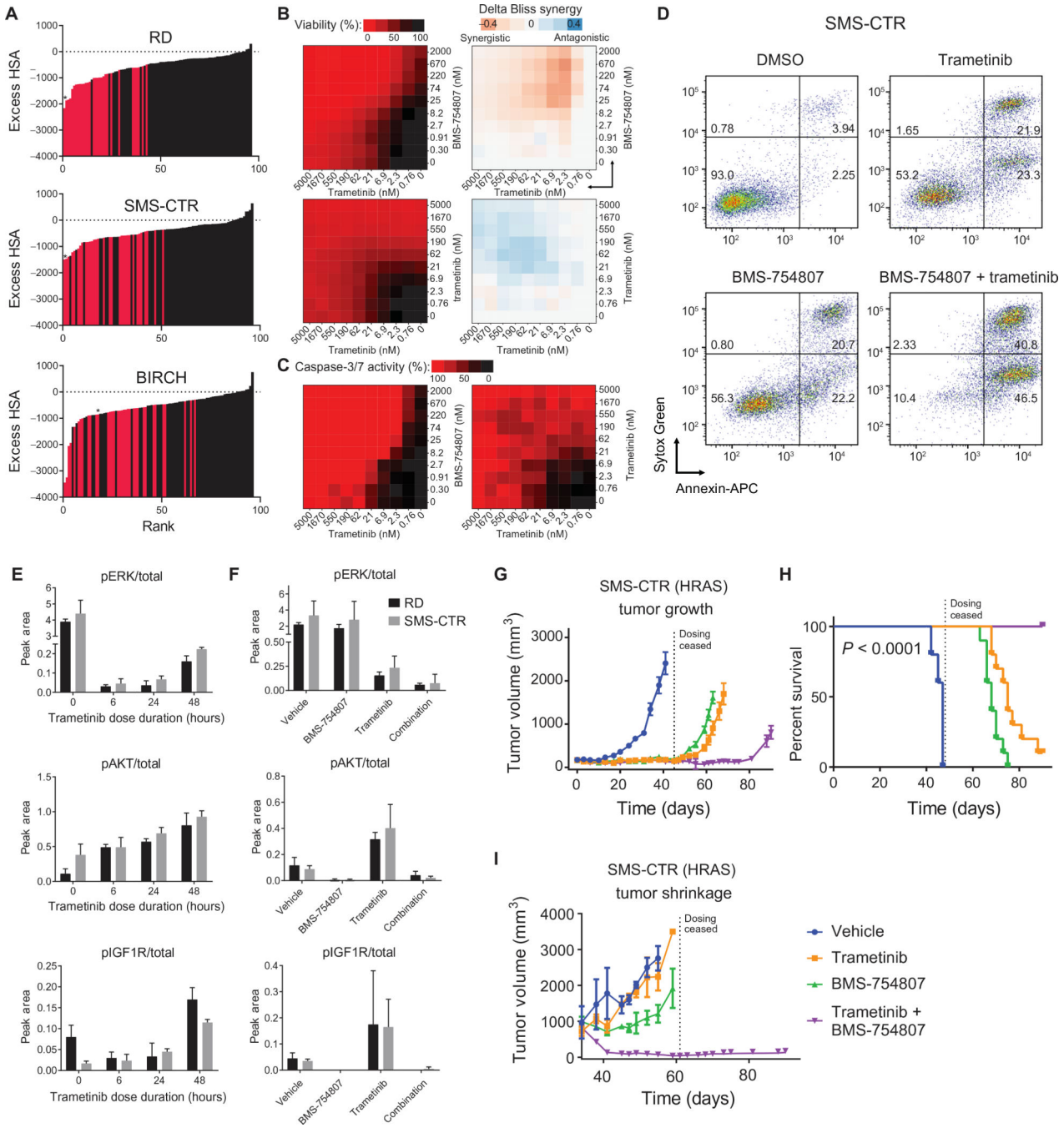

Fig. 7. Matrix screen identifies a synergistic combination of an IGF1R inhibitor and a MEK inhibitor in FN-RMS.

(**A**) Excess HSA versus rank plot representing 96 discreet synergy scores from the 10 × 10 matrix screen in RD, SMS-CTR, and BIRCH. Red bars indicate combinations of IGF1R/PI3K/mTOR/AKT and MEK/ERK inhibitors. Asterisk (*) denotes the combination of BMS-754807 and trametinib. (**B**) Matrix (10 × 10) plot for the combination of trametinib (0 to 5000 nM) and BMS-754807 (0 to 2000 nM) (top) or the control combination of trametinib with trametinib (bottom) in both viability (CellTiter-Glo; left) and ΔBliss (right) format. (**C**) Matrix (10 × 10) plot for caspase-3/7 activity of SMS-CTR treated for 16 hours

with the combination of trametinib and BMS-754807 (left) or the control combination of trametinib with trametinib (right). (**D**) Annexin V staining of SMS-CTR cells treated with DMSO, 100 nM trametinib, 350 nM BMS-754807, or the combination of trametinib and BMS-754807 for 72 hours. APC, allophycocyanin. (**E**) Peak area of the ratio of phosphorylated to total ERK (top), S473 AKT (middle), and IGF1R (bottom) as determined by Simple Western is displayed for RD (black) and SMS-CTR (gray) treated with 100 nM trametinib for the indicated times. (**F**) Peak area of the ratio of phosphorylated to total ERK (top), S473 AKT (middle), and IGF1R (bottom) as determined by Simple Western is displayed for RD (black) and SMS-CTR (gray) treated with DMSO or 100 nM trametinib for 72 hours, followed by DMSO or 350 nM BMS-754807 for 3 hours. (**G**) Daily treatment with the combination of trametinib and BMS-754807 prolongs the time to tumor development. Dotted line indicates date at which treatment was stopped (45 days). (**H**) Prolongation of survival in SMS-CTR xenografts either agent alone or combined ($P < 0.0001$, Mantel-Cox test for the comparison between single agent and the combination). (**I**) Daily treatment with the combination of trametinib and BMS-754807 in large established tumors induces regression in SMS-CTR xenografts. Dotted line indicates date at which treatment was stopped (28 days).